Philippine Journal of Science
151 (S1): 25-60, Marine Botany
ISSN 0031 - 7683
Date Received: 19 Apr 2021

α-Glucosidase Inhibitors from the Bark Extract of Ethno-Antidiabetic *Ceriops tagal* (Perr.) C.B. Rob

Bernard S. Canusa[1], **Ivan L. Lawag**[2,7], **Oliver B. Villaflores**[1,3,4], **Vitthal D. Wagh**[5], **Michal Korinek**[5,8,9], **Yi-Hong Tsai**[5], **Fang-Rong Chang**[5,10,11,12], and **Ma. Alicia M. Aguinaldo**[1,3,6*]

[1]The Graduate School
University of Santo Tomas, España Blvd. 1015 Manila, Philippines
[2]Chemistry Department, College of Science, Adamson University
900 San Marcelino Street, Ermita, Manila 1000 Philippines
[3]Research Center for the Natural and Applied Sciences
Thomas Aquinas Research Complex
University of Santo Tomas, España Blvd. 1015 Manila, Philippines
[4]Department of Biochemistry, Faculty of Pharmacy
University of Santo Tomas, España Blvd. 1015 Manila, Philippines
[5]Graduate Institute of Natural Products, College of Pharmacy
Kaohsiung Medical University, Kaohsiung 807 Taiwan
[6]Department of Chemistry, College of Science
University of Santo Tomas, España Blvd. 1015 Manila, Philippines
[7]Division of Pharmacy, School of Allied Health
Faculty of Health and Medical Sciences
University of Western Australia, 35 Stirling Highway, Crawley, WA 6009 Australia
[8]Graduate Institute of Natural Products, College of Medicine
Chang Gung University, Taoyuan 33302 Taiwan
[9]Research Center for Chinese Herbal Medicine
Research Center for Food and Cosmetic Safety, and
Graduate Institute of Health Industry Technology, College of Human Ecology
Chang Gung University of Science and Technology, Taoyuan 33302 Taiwan
[10]Drug Development and Value Creation Research Center
Kaohsiung Medical University, Kaohsiung 807 Taiwan
[11]Department of Medical Research, Kaohsiung Medical University Hospital
Kaohsiung Medical University, Kaohsiung 807 Taiwan
[12]Department of Marine Biotechnology and Resources
National Sun Yat-sen University, Kaohsiung 804 Taiwan

The bark of *Ceriops tagal* has been used in the Philippines for folk treatment of diabetes mellitus (DM). Through an α-glucosidase inhibition assay guided isolation, constituents from the detannified methanolic bark extract were isolated and identified to be methyl 2,4-dihydroxy-3,6-dimethyl benzoate (1), isopimar-7-ene-15S,16-diol (2), betulinic acid (3), lupeol (4), and methyl 2,4-dihydroxy-6-methyl benzoate (5). Compounds 3 (IC_{50} = 5.31 µM) and 4 (IC_{50} = 55.84 µM)

*Corresponding Author: amaguinaldo@ust.edu.ph

showed a more potent activity against α-glucosidase than the positive control, 1-deoxynojirimycin (IC_{50} = 79.16 µM). This is the first report on the presence of the weakly active compounds (1, 2, and 5) (IC_{50} > 75 µM) in the genus *Ceriops* and the first report on the biological activity of Compound 2. Enzyme kinetic studies suggested that betulinic acid is an uncompetitive type of inhibitor, with lupeol as a non-competitive type. This study provides evidence on the possible mechanism of the antidiabetic property of *C. tagal* associated with its traditional use. It supports the possible utilization of the bark for development to prevent or treat diabetes.

Keywords: α-glucosidase inhibitors, antidiabetic, betulinic acid, *Ceriops tagal*, lupeol, Rhizophoraceae

INTRODUCTION

DM is a chronic disease wherein there is an elevated blood glucose level or hyperglycemia for a prolonged period. Possible complications of DM are cardiovascular disease, nephropathy, neuropathy, and retinopathy (Ghani 2015). In 2019, 463 million adults (20–79 yr) worldwide were diagnosed with diabetes. In the Western Pacific region, the Philippines ranked fifth with 4.0 million adults diagnosed with DM with a prevalence of 6.3%. By 2045, the number of adults diagnosed with DM in the world is projected to increase to 700 million (IDF 2019).

One way of managing Type 2 DM is through the use of α-glucosidase inhibitors, which are oral antihyperglycemic drugs that reversibly inhibit intestinal α-glucosidases. These enzymes break down polysaccharides or disaccharides into glucose – thus inhibiting the activity of α-glucosidase, slowing down the absorption of carbohydrates, and resulting in a lowering of postprandial blood glucose (Marín-Peñalver *et al.* 2016). The use of α-glucosidase inhibitors is a relatively safer mode of treatment as compared to other antidiabetic agents due to its localized mode of action, minimal absorption, and low probability of systemic toxicity (Ghani 2015).

Mangrove plants are reported to be a rich source of natural products. Secondary metabolites obtained from mangroves and their derivatives are being used for managing DM around the world (Sachithanandam *et al.* 2019). *Ceriops tagal* (Perr.) C.B. Rob (Rhizophoraceae), locally known in the Philippines as "tangal," is a mangrove plant that is widely distributed from eastern Africa, tropical Asia, northern Australia to Melanesia, Micronesia, and southern China. This plant has been used as a source of tannins and as a traditional medicine for the treatment of a variety of diseases (Tsai *et al.* 2012). The bark of this plant was used as a folk treatment for diabetes in the Philippines (Santos *et al.* 1981) and for malignant ulcers and hemorrhage in India (Tiwari *et al.* 2008), while the leaves were used as a remedy to malaria in China (Wang *et al.* 2012). The leaf extract of *C. tagal* was reported to significantly improve glucose tolerance in normoglycemic sucrose-loaded rats and lowered blood glucose levels in streptozotocin-induced diabetic rats (Tiwari *et al.* 2008). In a previous study, the bark extract was reported to have a high inhibitory activity towards *α*-glucosidase (IC_{50} = 0.857 ± 1.46 µg mL^{-1}) (Lawag *et al.* 2012). In this study, the constituents responsible for the α-glucosidase inhibitory activity were isolated using a bioactivity-guided fractionation approach and identified using various spectroscopic methods. Moreover, the type of inhibition was determined.

METHODOLOGY

General Experimental Procedures

The α-glucosidase from *Saccharomyces cerevisiae* (yeast), p-nitrophenyl-α-D-glucopyranoside (p-NPG), and 1-deoxynojirimycin (positive control) were purchased from Sigma-Aldrich (United States). The reagents and solvents used are all analytical grade. Silica gel 60 (particle size 0.063–0.200 mm, Merck, Darmstadt, Germany) was used for column chromatography (CC). All the ^{1}H, ^{13}C, and 2D [correlation spectroscopy (COSY), heteronuclear single quantum coherence (HSQC), and heteronuclear multiple bond correlation (HMBC)] nuclear magnetic resonance (NMR) spectra were analyzed on a JEOL 400 NMR spectrometer. All the compounds were dissolved in $CDCl_3$ before NMR analysis. HPLC separation was done on a Waters 2695 Separation module and Zorbax Eclipse XDB-C18 Narrow Bore RR (2.1 x 150 mm x 3.5 µm) column eluted with 0.02% aqueous formic acid (mobile phase A) and 0.02% formic acid

in methanol (mobile phase B). The flow rate was 0.2 mL/min and the following gradient program was used: 5% B (2.5 min) and 100% B (50–100 min). The detector used was for electrospray ionization mass spectrometry (ESI-MS) (Waters micromassZQ).

Plant Material

The bark of *Ceriops tagal* (Perr.) C.B. Rob. was collected at Ivisan, Capiz, Philippines in May 2013 and identified by Dr. Wilfredo F. Vendivil, and a voucher specimen (USTH 5359) was deposited at the University of Santo Tomas Herbarium within the Botany Laboratory of the Research Center for the Natural and Applied Sciences.

Extraction and detannification. The powdered air-dried bark of *Ceriops tagal* (4.5 kg) was exhaustively extracted with 80% methanol in water, and a portion of the subsequent concentrated extract (100 g) was subjected to detannification according to the method described by Wall *et al.* (1996) with slight modification. It was dissolved in 90% methanol (400 mL) and partitioned with hexane (200 mL x3). The methanol layer was concentrated, diluted to 400 mL with water, and partitioned with ethyl acetate (EtOAc, 200 mL x5). The concentrated ethyl acetate extract (CtE, 3.9 g) was partitioned between methanol-dichloromethane-water (20:40:40, 200 mL) to obtain the lower layer, which was dried with anhydrous sodium sulfate and evaporated *in vacuo* (CtE 1) (0.88 g, 0.88% yield). CtE 1 showed negative to gelatin and ferric chloride tests, indicating complete removal of tannins. The detannified extract CtE1 was then subjected to separation.

Isolation of compounds. The detannified fraction, CtE 1 (786 mg), was fractionated by silica gel CC using DCM: EtOAc (20:0.1 to 5:5) to obtain 14 pooled fractions. The pooled fractions were tested for α-glucosidase inhibitory activity. The fractions CtE 1.3, 1.6, and 1.7 exhibited high activity with relatively good yield and, thus, were purified further (Appendix Table I).

Fraction CtE 1.3 (20.5 mg) was subjected to silica gel CC eluting with petroleum ether-EtOAc (98:2, 7:3) to obtain 14 sub-fractions. The major fraction CtE 1.3.7 (8.5 mg) was separated in silica gel CC with petroleum ether: acetone (15:1), obtaining semi-pure fractions CtE 1.3.7.5 (0.7 mg) and CtE 1.3.7.6 (1.5 mg), which were recrystallized using warm methanol to give Compound **1** (2.0 mg) as white crystals.

CtE 1.7 (23.7 mg) was purified by silica gel CC using petroleum ether: EtOAc (7:3, 1:9). The major fraction CtE 1.7.4 (10.9 mg) was chromatographed on silica [petroleum ether: EtOAc (8:2)] to give CtE 1.7.4.5 (4.5 mg), which was recrystallized in warm methanol to give Compound **2** (1.8 mg).

Recrystallization of CtE 1.6 (22.4 mg) with warm methanol yielded Compound **3** (2.6 mg).

For isolation of additional amounts of **1**, **2**, and **3**, the same detannification procedure was repeated on two portions of the crude extract (100.0 g each) that yielded the detannified extracts, Ct2E 1 (709 mg, 0.71% yield) and Ct3E 1 (505 mg, 0.51% yield). Similar separation procedures with CtE 1 were performed.

Compound **1** was re-isolated in subfractions Ct2E 1.4.2.2A (3.5 mg) and Ct3E 1.4.2.4.2 (3.6 mg). Compound **4** was co-isolated during the re-isolation of **1**. Silica gel CC of Ct2E 1.4 (24.2 mg) using hexane-EtOAc (9:1) gave subfraction Ct2E 1.4.2, which was iteratively purified to yield **4** (4.3 mg). Compound **4** was re-isolated from Ct3E 1.4 (22.6 mg) as Ct3E 1.4.2.2.2 (7.6 mg). Compound **2** (2.1 mg) was re-isolated from Ct2E 1.8 (68.1 mg) through repeated silica gel CC and preparative TLC. Re-isolation of **3** was done by fractionation of Ct2E 1.7 in a silica gel CC using hexane-EtOAc (8:2, 3:7). Recrystallization of Ct2E 1.7.3 (11.7 mg) by warm methanol yielded **3** (1.3 mg). Compound **5** (3.6 mg) was co-isolated in fraction Ct2E 1.7.2.

In Vitro* Inhibition Assay for α-Glucosidase from *Saccharomyces cerevisiae

The α-glucosidase inhibition assay method was adapted from the method of Lawag *et al.* (2012) with slight modification. In a 96-well plate, 140 µL of 100 mM phosphate buffer with 50 mM NaCl (pH 6.8), 15 µL of the samples/control (1000, 500, 250, 125, and 62.5 ppm), 15 µL of DMSO (dimethylsulfoxide) for the blank wells, and 20 µL α-glucosidase solution (0.017 units/well) were dispensed to the corresponding wells and was incubated for 15 min at 37 °C. Using a multi-channel micropipette, 25 µL of the substrate solution (0.7 mM) was added to each well and the absorbance was read at 405 nm (initial reading) in a 96-well plate reader. The microwell plate was incubated for 30 min at 37 °C. After incubation, the absorbance was read at 405 nm (final reading). The percent inhibition of the samples/control was calculated using the following formula:

$$\%\ Inhibition = \frac{\left(\left(Abs_{Blank\,(final)} - Abs_{Blank\,(initial)}\right) - \left(Abs_{Sample\,(final)} - Abs_{Sample\,(initial)}\right)\right)}{\left(Abs_{Blank\,(final)} - Abs_{Blank\,(initial)}\right)} x100 \quad (1)$$

The IC_{50} was obtained through linear regression of the concentration-response curve. Logarithmic transformation was done on the concentration (x), and the percent inhibition (y) was transformed to the logit parameter. Logit transformation of the percent inhibition was done using the following equation:

$$logit\ (P) = ln\left(\frac{P}{100\% - P}\right) \quad (2)$$

where *P* is the percent inhibition of the inhibitor (Miyata *et al.* 2016). Plotting the logit against the logarithm of the concentration resulted in a straight line and by linear regression, the IC_{50} was determined.

Enzyme Kinetic Analysis

The enzyme kinetic analysis of Compounds **3** and **4** was done using the same method for the determination of α-glucosidase activity described in the previous section. Different concentrations of p-NPG (1.4, 0.7, 0.35, and 0.175 mM) were used. The absorbance was read at 0, 5, 10, 15, 20, 25, and 30 min. The mode of inhibition was determined by analyzing the Lineweaver-Burk plot.

Data were statistically calculated by two-way analysis of variance (ANOVA), followed by Bonferroni's test using GraphPad Prism version 6.01 (United States). The values were considered significant when $p < 0.05$.

RESULTS AND DISCUSSION

The mangrove bark is a rich source of tannins and polyphenols (Sachithanandam *et al.* 2019). Tannins are large molecules that can interact with proteins, forming a water-insoluble complex. For this reason, tannins are reported to interfere with enzyme-based assays (Wall *et al.* 1996) and in the purification process. Thus, the detannification of tannin-rich extracts is essential before performing assays in order to avoid false-positive results (Krasteva *et al.* 2011) and to facilitate purification. The modified detannification process of the crude extract yielded the dichloromethane extract (CtE 1, 81% inhibition at 75 µg/mL), which – from the dose-response curve obtained at different dilutions of the extract – gave the IC_{50} value of 40.16 ug/mL.

α-Glucosidase Inhibition Profiling

To determine the active constituents responsible for the α-glucosidase inhibitory activity of CtE 1, the constituents were separated using silica gel CC, resulting in 14 pooled fractions. The α-glucosidase inhibition assay of the 14 subfractions exhibited differences in activities (Figure 1). High inhibitory activity was observed at the less polar fractions (1.2. 1.3, and 1.5–1.9), while the more polar fractions (1.10–1.14) showed no inhibition of α-glucosidase. The active fractions were further separated and purified, obtaining compounds **1–5**.

Identification of Compounds 1–5

Five compounds were isolated through a series of silica gel chromatographic separations. Their structures were elucidated using a combination of 1D NMR, 2D NMR (COSY, HMQC, and HMBC), and ESI-MS. Comparison of their spectroscopic data with literature showed the compounds to be methyl 2,4-dihydroxy-3,6-dimethyl benzoate (**1**) (Nishiyama *et al.* 2018), isopimar-7-ene-15S,16-diol (**2**) (Li *et al.* 1991), betulinic acid (**3**) (Dais *et al.* 2017), lupeol (**4**) (Beserra *et al.* 2018), and methyl 2,4-dihydroxy-6-methyl benzoate (**5**) (Basset *et al.* 2010) (Figure 2). Of these, Compounds **1, 2,** and **5** were isolated for the first time in *C. tagal*. The detailed spectroscopic data for Compounds **1–5** can be found in the Appendices section.

Compounds **1** and **5** showed characteristic features of an aromatic compound at δ_C100.0-160.0, with an acyl moiety at δ_C172.6, acyloxymethyl at δ_C 51.8, with evidence of hydroxyls at δ_C 158.0 and 163.1, and benzylic methyl at δ_H 2.10 and 2.46. The difference lies only in the presence of an additional benzylic methyl for Compound **1**.

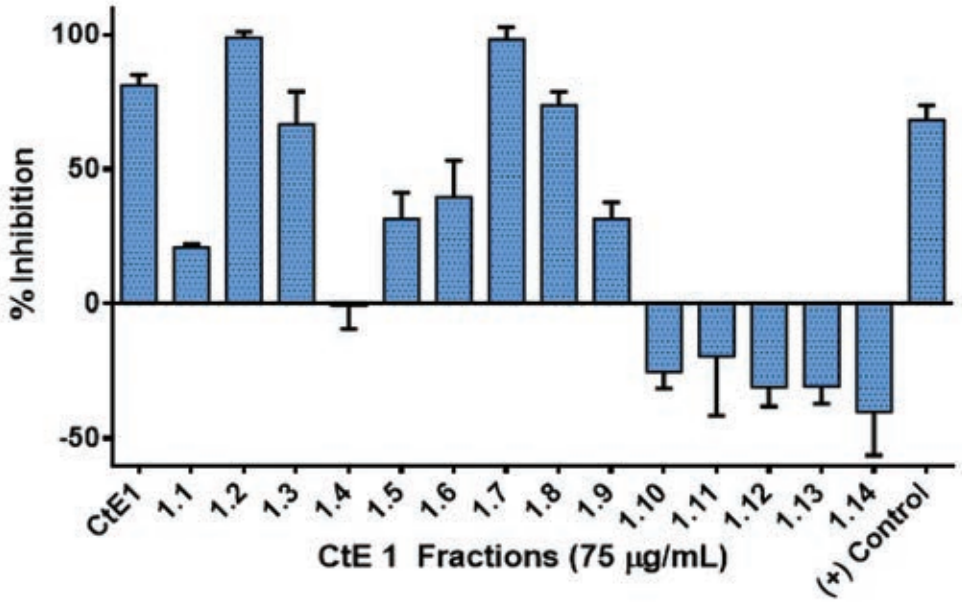

Figure 1. α-Glucosidase Inhibitory activity of CtE 1 fractions. The values are reported as mean ± SD of n = 3 replicates.

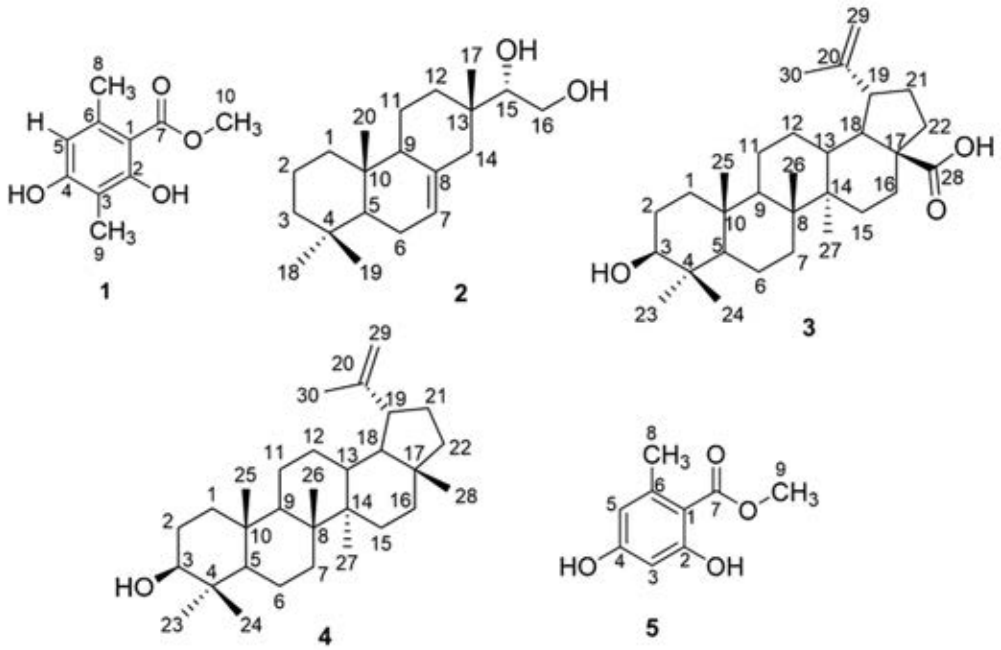

Figure 2. Structures of Compounds **1–5**.

Compound **2** exhibited spectroscopic features of a tricyclic diterpenoid of the pimarane type, possessing hydroxyls at the side chain at C-15 and C-16 (δ_H 3.69, 3.49) plus characteristic double bond at position 7(8) (δ_C 122.4, 135.3) and four methyls (δ_H 0.82–0.91) for C-17, C-18, C-19, and C-20.

Compounds **3** and **4** are pentacyclic triterpenoids of the lupane type, with a characteristic double bond at position 20(29) (δ_C 150.4, 109.7) and 3δ-hydroxy substituent (δ_H 3.2). Compound **3** has a carboxylic acid (δ_C180.1) for position 29, while Compound **4** has a methyl (δ_C 18.0) for this position.

Of these, Compounds **1, 2,** and **5** were isolated for the first time in *C. tagal*. Compound **3** was previously isolated from the hypocotyls and fruits of *C. tagal* (Yu *et al.* 2014), while Compound **4** was isolated from the roots and aerial parts (Ríos and Máñez 2018). The diterpenoid 15(S)-isopimar-7-ene-15,16-diol (**2**) was previously isolated from the root bark and stems of the mangrove plant *Bruguiera gymnorrhiza* (Rhizophoraceae) (Nishiyama *et al.* 2018). To this date, this is the first report on the isolation and identification of 2,4-dihydroxy-3,6-dimethyl methylbenzoate (**1**), 15(*S*)-isopimar-7-ene-15,16-diol (**2**), and 2,4-dihydroxy-6-methyl methylbenzoate (**5**) in the genus *Ceriops* (Rhizophoraceae).

Compound **3** was previously isolated from the hypocotyls and fruits of *C. tagal* (Pakhathirathien *et al.* 2005), while Compound **4** was isolated from the roots and aerial parts (Chacha 2005). The diterpenoid 15(S)-isopimar-7-ene-15,16-diol (**2**) was previously isolated from the root bark and stems of the mangrove plant *Bruguiera gymnorrhiza* (Rhizophoraceae) (Subrahmanyam *et al.* 1999). To this date, this is the first report on the isolation and identification of 2,4-dihydroxy-3,6-dimethyl methylbenzoate (**1**), 15(*S*)-isopimar-7-ene-15,16-diol (**2**), and 2,4-dihydroxy-6-methyl methylbenzoate (**5**) in the genus *Ceriops* (Rhizophoraceae).

α-Glucosidase Inhibitory Activity of Compounds 1–5

The result of the α-glucosidase inhibitory activity assay showed betulinic acid (**3**) and lupeol (**4**) to exhibit high inhibitory activity. The dose-response curves of Compounds **3** and **4** at different dilutions revealed the IC_{50} as 5.31 and 55.84 µM, respectively, with Compound **3** being 19 times more potent than the standard 1-deoxynojirimycin (IC_{50} = 79.16 µM). These results agree with the literature for betulinic acid (IC_{50} = 7.8 µM) (Gundoju *et al.* 2018) and lupeol (IC_{50} = 71.2 µM) (Yu *et al.* 2014). On the contrary, Compounds **1** (IC_{50} > 382.3 µM), **2** (IC_{50} > 244.7 µM), and **5** (IC_{50} > 411.9 µM) showed very weak to no inhibitory activity against α-glucosidase (Figure 3).

Betulinic acid (**3**) and lupeol (**4**) are known to be biologically active compounds. Betulinic acid (**3**) was reported to exhibit adenosine monophosphate-activated protein kinase activation, which increases the transport of glucose across the cell membrane, and inhibition of protein tyrosine phosphatase 1B (PTP1B). It also showed increased glycogen content and glucose uptake in muscle in hyperglycemic rats by acting as an insulin secretagogue and insulin-mimetic agent in these pathways: phosphoinositide-3-kinase, mitogen-activated protein kinase, and mRNA translation (Ríos and Máñez 2018).

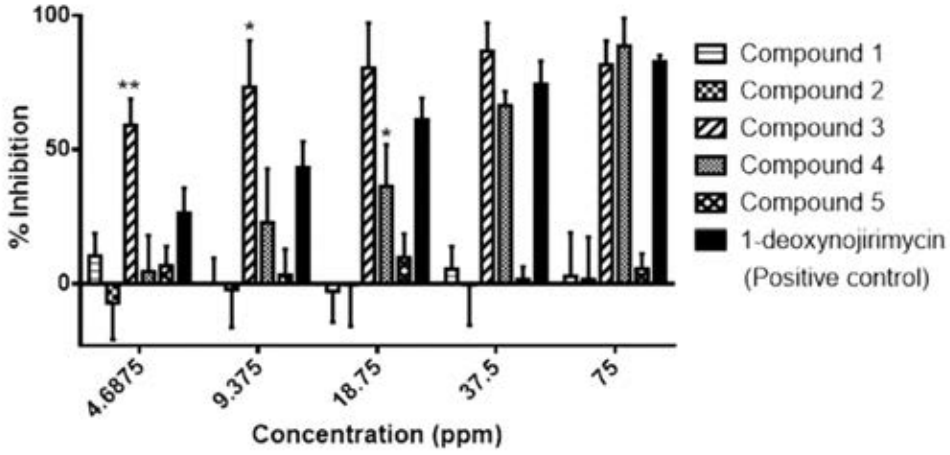

Figure 3. Percent inhibition of a-glucosidase by Compounds 1–5 and 1-deoxynojirimycin. The values are reported as mean ± SE of n = 3 experiments performed in triplicate. Significant differences to the positive control (ANOVA/Bonferroni) are indicated by: *$p < 0.05$; **$p < 0.01$.

Lupeol (**4**) was also reported to exhibit PTB1B inhibitory activity (Siddique and Saleem 2011) and prevent the development of streptozotocin-induced diabetes in rats after 21 d (Gupta *et al.* 2012). Lupeol and lupeol ester derivatives showed an anti-hyperglycemic effect on sucrose-loaded streptozotocin-induced diabetic rats (Lakshmi *et al.* 2014).

Compounds **1** and **5** were commonly isolated from lichens, in which most of the secondary metabolites comprise phenolic compounds that are known for their antioxidant activity (Shukla *et al.* 2010). Methyl 2,4-dihydroxy-6-methylbenzoate (**5**) was reported to exhibit antidiabetic activity through PTP1B inhibition in a dose-dependent manner (IC_{50} = 277 ± 8.6 µM), leading to an increase in insulin sensitivity (Seo *et al.* 2009). These activities may also contribute to the antidiabetic activity of *Ceriops tagal*.

Synergistic inhibitory activity assay was not done in the study. However, a few interesting observations were noted. Fraction CtE 1.7 showed good inhibitory activity (98.4%) as compared to the isolated compound from this fraction (**2**), which showed very weak to no inhibitory activity. This indicates that other components may have an inhibitory activity or may have a synergistic effect with Compound **2**. For Compound **3**, the pure compound showed higher inhibitory activity (81.7%) than the fraction where it was isolated, CtE 1.6 (39.7%). Compound **5**, which was co-isolated in the same fraction as Compound **3**, exhibited very weak to no inhibitory activity, suggesting that there is no synergistic effect between Compounds **3** and **5**. Fraction CtE 1.3 exhibited good inhibitory (66.9%) as compared to Compound **1** isolated from this fraction, which has very weak to no inhibitory activity. Compound **4**, which was co-isolated from the same fraction as Compound **1**, exhibited high inhibitory activity (88.6%), suggesting that there is no synergistic effect between Compounds **1** and **4**.

Mode of Inhibition of Compounds 3 and 4

The inhibition mechanisms of the active compounds (**3** and **4**) were determined using the Lineweaver-Burk plot (Figure 4). When the concentration of Compound **3** was increased, the maximum rate (V_{max}) decreased, which is observed from the rise of the y-intercept. The decrease in the value of the Michaelis-Menten constant (K_M) was also observed, as represented by the shifting of the x-intercept to the left. It can be inferred from these observations that Compound **3** inhibited α-glucosidase through an uncompetitive type mechanism. In comparison with the previous investigations, Ding *et al.* (2018) reported betulinic acid to exhibit a mixed type of inhibition, while López *et al.* (2015) reported it as a competitive type. Both studies did a docking simulation of betulinic acid with α-glucosidase, agreeing that betulinic acid binds with the active site of α-glucosidase by hydrophobic interactions. The results of this study provide a different insight into how betulinic acid interacts with α-glucosidase through uncompetitive inhibition. This may prove to be significant as uncompetitive inhibitors will increase in potency as the substrate concentration increases in contrast with competitive inhibitors, which tend to behave otherwise (Cornish-Bowden 1986). For this reason, uncompetitive inhibitors are considered superior for drug development compared to noncompetitive and competitive inhibitors and are expected to be more efficient *in vivo* (Song *et al.* 2016).

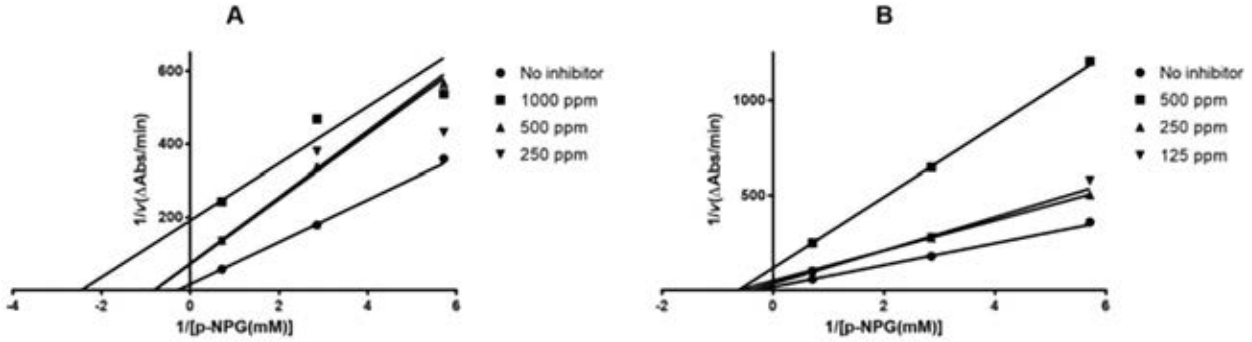

Figure 4. Lineweaver-Burk plots of betulinic acid (A) and lupeol (B). The values are reported from trial (n = 1).

Inspection of the Lineweaver-Burk plot of Compound **4** shows a rise in the slope as the concentration of the inhibitor was increased, corresponding to the decrease of the V_{max} of the enzyme. It was also observed that the lines approximately meet at the same point in the x-axis, signifying that the affinity of the enzyme to the substrate (K_M) did not change much. From these data, it can be concluded that Compound **4** inhibited α-glucosidase by a non-competitive type mechanism. The observed noncompetitive inhibition of lupeol agreed with the previous report of Ramu *et al.* (2014).

CONCLUSION

The present study isolated and identified methyl 2,4-dihydroxy-3,6-dimethyl benzoate (**1**), isopimar-7-ene-15S,16-diol (**2**), betulinic acid (**3**), lupeol (**4**), and methyl 2,4-dihydroxy-6-methyl benzoate (**5**) from the detannified methanol bark extract of the ethno-antidiabetic *Ceriops tagal* through bioassay-guided isolation. The very active α-glucosidase inhibitors (betulinic acid and lupeol) exhibited a more potent activity than the positive control (1-deoxynojirimycin). This is the first report on the presence of the weakly active compounds (**1**, **2**, and **5**) in the genus *Ceriops* and the first report on the biological activity of Compound **2**. Enzyme kinetic analysis of betulinic acid and lupeol demonstrated uncompetitive and noncompetitive types of inhibitors, respectively. This research substantiates the previous results assessing the effects of *C. tagal* bark extract on α-glucosidase activity and provides a possible mechanism on its antidiabetic property associated with its traditional use in the Philippines. Further, it proves that the bark of the mangrove plant *Ceriops tagal* may be considered a rich source of α-glucosidase inhibitors that are worth developing for the prevention and/or treatment of diabetes.

ACKNOWLEDGEMENT

This work was supported by the Science Education Institute of the Philippine Department of Science and Technology.

NOTE ON APPENDICES

The complete appendices section of the study is accessible at http://philjournsci.dost.gov.ph

REFERENCES

ANJANEYULU A, RAO V. 2002. Ceriopsins A–D, diterpenoids from *Ceriops decandra*. Phytochemistry 60: 777–782.

BASSET J, LESLIE C, HAMPRECHT D, WHITE AJ, BARRETT AG. 2010. Studies on the resorcylates: biomimetic total syntheses of (+)-montagnetol and (+)-erythrin. Tetrahedron Lett. 51: 783–785.

BESERRA FP, XUE M, MAIA G, ROZZA AL, PELLIZZON CH, JACKSON CJ. 2018. Lupeol, a Pentacyclic Triterpene, Promotes Migration, Wound Closure, and Contractile Effect *In Vitro*: Possible Involvement of PI3K/Akt and p38/ERK/MAPK Pathways. Molecules 23: 2819–2835.

CHACHA M. 2005. Terpenoids from the roots of *Ceriops tagal* induces apoptosis through activation of caspase-3 enzyme. Int J Biol Chem Sci 5: 402–409.

CORNISH-BOWDEN A. 1986. Why is uncompetitive inhibition so rare? FEBS Lett 203: 3–6.

DAIS P, PLESSEL R, WILLIAMSON K, HATZAKIS E. 2017. Complete ^{1}H and ^{13}C NMR assignment and ^{31}P NMR determination of pentacyclic triterpenic acids. Anal Methods 9: 949–957.

DING H, WU X, PAN J, HU X, GONG D, ZHANG G. 2018. New insights into the inhibition mechanism of betulinic acid on α-Glucosidase. J Agric Food Chem 66: 7065–7075.

GHANI U. 2015. Re-exploring promising α-glucosidase inhibitors for potential development into oral antidiabetic drugs: finding needle in the haystack. Eur J Med Chem 103: 133–162.

GUNDOJU N, BOKAM R, YALAVARTHI NR, AZAD R, PONNAPALLI MG. 2018. Betulinic acid derivatives: a new class of α-glucosidase inhibitors and LPS-stimulated nitric oxide production inhibition on mouse macrophage RAW 264.7 cells. Nat Prod Res 33: 2618–2622.

GUPTA R, SHARMA AK, SHARMA M, DOBHAL M, GUPTA R. 2012. Evaluation of antidiabetic and antioxidant potential of lupeol in experimental hyperglycaemia. Nat Prod Res 26: 1125–1129.

[IDF] International Diabetes Federation. 2019. Diabetes Atlas, 9th edition. Retrieved on 4 Dec 2019 from https://diabetesatlas.org/

KRASTEVA S, HEISS E, KRENN L. 2011. Optimization and application of a fluorimetric assay for the identification of histone deacetylase inhibitors from plant origin. Pharm Biol 49: 658–668.

LAKSHMI V, MAHDI AA, AHMAD MK, AGARWAL SK, SRIVASTAVA AK. 2014. Antidiabetic Activity of Lupeol and Lupeol Esters in Streptozotocin-induced Diabetic Rats. Bangladesh Pharm J 17: 138–146.

LAWAG I, AGUINALDO A, NAHEED S, MOSIHUZZAMAN M. 2012. α-Glucosidase inhibitory activity of selected Philippine plants. J Ethnopharmacol 144: 217–219.

LI C, LIN Z, ZHENG H, ZHANG H, SUN H. 1991. The chemical constituents of *Coleus esquirolii*. Chin Chem Lett 2: 223–226.

LÓPEZ D, CHERIGO L, SPADAFORA C, LOZA-MEJÍA M, MARTÍNEZ-LUIS S. 2015. Phytochemical composition, antiparasitic and α–glucosidase inhibition activities from *Pelliciera rhizophorae.* Chem Cent J 9: 1–11.

MARÍN-PEÑALVER JJ, MARTÍN-TIMÓN I, SEVILLANO-COLLANTES C, CAÑIZO-GÓMEZ FJD. 2016. Update on the treatment of type 2 diabetes mellitus. World J Diabetes 7*:* 354–395.

MIYATA KI, NAKAGAWA Y, KIMURA Y, UEDA K, AKAMATSU M. 2016. Structure-activity relationships of dibenzoylhydrazines for the inhibition of P-glycoprotein-mediated quinidine transport. Bioorg Med Chem 24: 3184–3191.

NISHIYAMA Y, NODA Y, NAKATANI N, SHITAN N, SUDO T, KATO A, MUTISO PBC. 2018. Structure of constituents isolated from the bark of *Cassipourea malosana* and their cytotoxicity against a human ovarian cell line. J Nat Med 73: 289–296.

PAKHATHIRATHIEN C, CHANTRAPROMMA S, FUN H, ANJUM S, RAHMAN A, KARALAI C. 2005. 1-Isopropenyl-3a,5a,5b,8,8,11a-hexamethylicosahydro-1H-cyclopenta[a]chrysen-9-yl-4-hydroxy-3-methoxycinnamate. Acta Crystallogr Sect E 61: 2942–2944.

RAMU R, SHIRAHATTI PS, ZAMEER F, RANGANATHA LV, PRASAD MN. 2014. Inhibitory effect of banana (*Musa* sp. var. Nanjangud rasa bale) flower extract and its constituents umbelliferone and lupeol on α-glucosidase, aldose reductase and glycation at multiple stages. S Afr J Bot 95: 54–63.

RÍOS J, MÁÑEZ S. 2018. New Pharmacological Opportunities for Betulinic Acid. Planta Med 84: 8–19.

SACHITHANANDAM V, LALITHA P, PARTHIBAN A, MAGESWARAN T, MANMADHAN K, SRIDHAR R. 2019. A Review on Antidiabetic Properties of Indian Mangrove Plants with Reference to Island Ecosystem. Evid Based Complement Alternat Med. p. 1–21.

SANTOS AC, SANTOS GA, OBLIGACION MB, OLAY LP, FOJAS FR. 1981. Philippine plants and their contained natural products and their pharmaceutical literature survey. National Research Council of the Philippines, Taguig City, Philippines.

SEO C, CHOI YH, AHN JS, YIM JH, LEE HK, OH H. 2009. PTP1B inhibitory effects of tridepside and related metabolites isolated from the Antarctic lichen *Umbilicaria antarctica.* J Enzym Inhib Med Ch 24: 1133–1137.

SHUKLA V, JOSHI GP, RAWAT MSM. 2010. Lichens as a potential natural source of bioactive compounds: a review. Phytochem Rev 9: 303–314.

SIDDIQUE HR, SALEEM M. 2011. Beneficial health effects of lupeol triterpene: a review of preclinical studies. Life Sci 88: 285–293.

SONG YH, KIM DW, CURTIS-LONG MJ, PARK C, SON M, KIM JY, YUK HJ, LEE KW, PARK KH. 2016. Cinnamic acid amides from *Tribulus terrestris* displaying uncompetitive α-glucosidase inhibition. Eur J Med Chem 114: 201–208.

SUBRAHMANYAM C, RAO BV, WARD RS, HURSTHOUSE MB, HIBBS DE. 1999. Diterpenes from the marine mangrove *Bruguiera gymnorhiza*. Phytochemistry 51: 83–90.

TIWARI P, TAMRAKAR A, AHMAD R, SRIVASTAVA M, KUMAR R, LAKSHMI V, SRIVASTAVA AK. 2008. Antihyperglycaemic activity of *Ceriops tagal* in normoglycaemic and streptozotocin-induced diabetic rats. Med Chem Res 1: 74–84.

TSAI C, LI S, SU Y, YONG JW, SAENGER P, CHESSON P, SHEUE C. 2012. Molecular phylogeny and evidence for natural hybridization and historical introgression between *Ceriops* species (Rhizophoraceae). Biochem Syst Ecol 43: 178–191.

URONES J, MARCOS I, DIEZ D, CUBILLA L. 1998. Tricyclic diterpenes from *Hyptys dilatata*. Phytochemistry 48(6): 1035–1038.

WALL M, WANI M, BROWN D, FULLAS F, OLWALD J, JOSEPHSON F, KINGHORN A. 1996. Effect of tannins on screening of plant extracts for enzyme inhibitory activity and techniques for their removal. Phytomedicine 3: 281–285.

WANG H, LI M, WU J. 2012. Chemical constituents and some biological activities of plants from the genus *Ceriops*. Chem Biodivers 9: 1–11.

YU MH, SHI ZF, YU BW, PI EH, WANG HY, HOU AJ, LEI C. 2014. Triterpenoids and α-glucosidase inhibitory constituents from *Salacia hainanensis*. Fitoterapia 98: 143–148.

APPENDIX I

^{1}H, ^{13}C NMR, and ESI-MS data of Compounds 1–5

Methyl 2,4-dihydroxy-3,6-dimethyl benzoate **(1)** – white crystal: ESIMS *m/z* 196.9 $[M+H]^+$; ^{1}H NMR ($CDCl_3$, 400 MHz) δ: 2.10 (3*H*, s, H-8), 2.46 (3H, s, H-9), 3.91 (3H, s, H-10), 5.25 (1H, br s, OH-4), 6.21 (1H, s, H-5), 12.03 (1H, s, OH-2); ^{13}C NMR ($CDCl_3$, 100 MHz) δ: 105.2 (C-1), 163.1 (C-2), 108.5 (C-3), 158.0 (C-4), 110.5 (C-5), 140.1 (C-6), 172.6 (C-7), 7.6 (C-8), 24.1 (C-9), 51.8 (C-10).

15(*S*)-Isopimar-7-ene-15,16-diol **(2)** – white crystal: ESIMS *m/z* 307.2 $[M+H]^+$; ^{1}H NMR ($CDCl_3$, 400 MHz) δ: 0.82 (3H, s, H-17), 0.83 (3H, s, H-20), 0.91 (3H, s, H-19), 0.87 (3H, s, H-18), 3.49 (1H, H-16), 3.69 (1H, H-15), 5.45 (1H, dd, *J*=5.6, 2.4 Hz, H-7); ^{13}C NMR ($CDCl_3$, 100 MHz) δ: 39.8 (C-1), 18.8 (C-2), 42.5 (C-3), 32.8 (C-4), 50.4 (C-5), 23.4 (C-6), 122.4 (C-7), 135.3 (C-8), 51.7 (C-9), 35.5 (C-10), 20.0 (C-11), 35.1 (C-12), 36.5 (C-13), 45.4 (C-14), 72.9 (C-15), 62.3 (C-16), 22.7 (C-17), 33.6 (C-18), 22.3 (C-19), 15.0 (C-20).

Betulinic acid **(3)** – white crystal: ESIMS *m/z* 935.3 $[2M+Na]^+$, 439.3 $[M+H-H_2O]^+$; ^{1}H NMR ($CDCl_3$, 400 MHz) δ: 0.75 (3H, s, H-23), 0.82 (3H, s, H-25), 0.93 (3H, s, H-26), 0.96 (3H, s, H-24), 0.97 (3H, s, H-27), 1.69 (3H, s, H-30), 3.20 (1H, dd, *J*=11.2, 4.8 Hz, H-3), 4.60 (1H, dd, *J*=2.0, 1.6 Hz, H-29a), 4.73 (1H, d, *J*=2.0 Hz, H-29b); ^{13}C NMR ($CDCl_3$, 100 MHz) δ: 38.7 (C-1), 27.4 (C-2), 79.0 (C-3), 38.9 (C-4), 55.3 (C-5), 18.3 (C-6), 34.3 (C-7), 40.7 (C-8), 50.5 (C-9), 37.2 (C-10), 20.8 (C-11), 25.5 (C-12), 38.4 (C-13), 42.4 (C-14), 29.7 (C-15), 32.1 (C-16), 56.3 (C-17), 49.3 (C-18), 46.9 (C-19), 150.4 (C-20), 37.0 (C-21), 30.5 (C-22), 27.9 (C-23), 15.3 (C-24), 16.1 (C-25), 16.0 (C-26), 14.7 (C-27), 180.1 (C-28), 109.7 (C-29), 19.4 (C-30).

Lupeol **(4)** – white crystal: ESIMS *m/z* 875.5 $[2M+Na]^+$, 409.3 $[M+H-H_2O]^+$; ^{1}H NMR ($CDCl_3$, 400 MHz) δ: 0.76 (3H, s, H-24), 0.79 (3H, s, H-28), 0.83 (3H, s, H-25), 0.94 (3H, s, H-27), 1.03 (3H, s, H-26), 1.68 (3H, s, H-30), 3.21 (1H, H-3), 4.56 (1H, H-29a), 4.68 (1H, H-29b); ^{13}C NMR ($CDCl_3$, 100 MHz) δ: 38.8 (C-1), 27.4 (C-2), 79.0 (C-3), 38.9 (C-4), 55.3 (C-5), 18.3 (C-6), 34.3 (C-7), 40.8 (C-8), 50.4 (C-9), 37.2 (C-10), 20.9 (C-11), 25.1 (C-12), 38.0 (C-13), 42.8 (C-14), 27.4 (C-15), 35.6 (C-16), 43.0 (C-17), 48.3 (C-18), 48.0 (C-19), 151.0 (C-20), 29.8 (C-21), 40.0 (C-22), 28.0 (C-23), 15.4 (C-24), 16.1 (C-25), 16.0 (C-26), 14.5 (C-27), 18.0 (C-28), 109.3 (C-29), 19.3 (C-30).

Methyl 2,4-dihydroxy-6-methyl benzoate **(5)** – white crystal: ESIMS *m/z* 182.9 $[M+H]^+$; ^{1}H NMR ($CDCl_3$, 400 MHz) δ: 2.49 (3H, s, H-8), 3.92 (3H, s, H-9), 5.36 (1H, s, OH-4), 6.22 (1H, dd, *J*=2.4, 0.8 Hz, H-5), 6.28 (1H, d, *J*=2.8 Hz, H-3), 11.74 (1H, s, OH-2); ^{13}C NMR ($CDCl_3$, 100 MHz) δ: 105.7 (C-1), 165.3 (C-2), 101.2 (C-3), 160.2 (C-4), 111.3 (C-5), 144.0 (C-6), 172.1 (C-7), 24.3 (C-8), 51.9 (C-9).

APPENDIX II

Table I. Weight and % inhibition of CtE 1 fractions.

Fraction	Weight (mg)	% inhibition (mean ± SD, n = 3) (75 µg/mL)
CtE 1	786	–
CtE 1.1	3.4	20.95 ± 1.15
CtE 1.2	3.3	99.00 ± 2.18
CtE 1.3	21.9	66.85 ± 12.14
CtE 1.4	36.6	–0.74 ± 8.48
CtE 1.5	15.5	31.57 ± 9.85
CtE 1.6	22.4	39.67 ± 13.55
CtE 1.7	24.9	98.44 ± 4.63
CtE 1.8	22.4	73.79 ± 5.15
CtE 1.9	48.3	31.52 ± 6.19
CtE 1.10	50.6	–25.25 ± 6.01
CtE 1.11	59.8	–19.33 ± 22.09
CtE 1.12	204.3	–30.81 ± 7.16
CtE 1.13	75.8	–30.57 ± 6.45
CtE 1.14	152.3	–40.09 ± 16.10

Table II. Comparison of ^{1}H and ^{13}C chemical shifts of (**1**) with methyl 2,4-dihydroxy-3,6-dimethyl benzoate.

	^{1}H chemical shift ($CDCl_3$, 400 MHz)	**^{1}H chemical shift ($CDCl_3$, 500 MHz)***	**^{13}C chemical shift ($CDCl_3$, 100 MHz)**	**^{13}C chemical shift ($CDCl_3$, 125 MHz)***
1			105.2	105.2
2			163.1	163.7
3			108.5	108.5
4			158.0	158.1
5	6.21, s	6.21, s	110.5	110.5
6			140.1	140.1
7	2.46, s	2.45, s	24.1	24.1
8			172.6	172.6
9	3.91, s	3.92, s	51.8	51.8
10	2.10, s	2.10, s	7.6	7.7
	12.03, s, 2-OH	12.01, s, OH		
	5.25, br s, 4-OH	5.28, br s, OH		

*Chemical shifts according to Nishiyama *et al*. (2018)

Table III. Comparison of ^{1}H and ^{13}C chemical shifts of (**2**) and 15*S*-isopimar-7-ene-15,16-diol / esquirolin B and ceriopsin C.

	^{1}H chemical shift (δ_H) ($CDCl_3$, 400 MHz)	^{13}C chemical shift (δ_C) ($CDCl_3$, 100 MHz)	^{1}H chemical shift (δ_H) ($CDCl_3$, 400 MHz)[a]	^{13}C chemical shift (δ_C) ($CDCl_3$, 100 MHz)[a]	^{1}H chemical shift (δ_H) ($CDCl_3$, 400 MHz)[b]	^{13}C chemical shift (δ_C)* ($CDCl_3$, 100 MHz)[b]	^{1}H chemical shift (δ_H) ($CDCl_3$, 400 MHz)[c]	^{13}C chemical shift (δ_C)* ($CDCl_3$, 100 MHz)[c]
1	0.98, dt, J=12.8, 3.2 Hz; 1.77, ddd, J=12.8, 4.8, 2.0 Hz	39.8		39.8		39.8	3.43, dd (10.8, 4.5 Hz)	81.5
2	1.45, m	18.8		18.8		18.8	1.62, m; 1.25, m	29.6
3	1.18, m	42.5		42.3		42.7	1.28, m; 1.45, m	40.0
4		32.8		32.5		32.8		32.7
5	1.13, m	50.4		50.4		50.3	1.10, m	50.1
6	1.92, m	23.4		23.4		19.5	1.50, m; 1.96, m	23.2
7	5.45, dd, J=5.6, 2.4 Hz	122.4	5.34, m	121.8	5.3, m	122.6	5.47, br s	122.1
8		135.3		135.4		134.2		136.0
9		51.7		51.9		52.0	1.95, m	52.1
10		35.5		35.4		37.0		41.2
11		20.0		19.9		23.5	2.15, m; 1.32, m	23.6
12		35.1		35.1		33.2	1.26, m; 1.60, m	35.5
13		36.5		36.4		35.4		36.4
14	2.44, dd, J=14, 2.8 Hz; 1.63, m	45.4		45.1		42.3	1.64, m; 2.45, m	46.0
15	3.69, m	72.9	3.70, dd, J=10.6, 11.5 Hz	73.1	4.91, dd, J = 2.5, 9.1 Hz	78.5	3.72, dd (10.5, 3 Hz)	72.7
16	3.49, m	62.3	3.64 dd, J=10.0, 11.5 Hz; 3.50 dd, J=10.0, 10.6 Hz	62.7	4.41, dd, J=2.5, 11.8 Hz; 4.01, dd, J=9.1, 11.8 Hz	63.2	3.47, dd (10.5, 9.5 Hz); 3.68, dd (9.5, 3.0 Hz)	62.3
17	0.82, s	22.7	0.80, s; 0.84, s; 0.86, s; 0.91, s	23.3	0.91, 3H, s; 0.86, 3H, s; 0.84, 6H, s	17.8	0.81, s	22.6
18	0.87, s	33.6		33.6		33.6	0.86, s	33.2
19	0.91, s	22.3		23.1		22.3	0.90, s	22.3
20	0.83, s	15.0		15.0		14.9	0.86, s	8.5
OOCMe						171.0, 170.6, 20.9, 20.8		

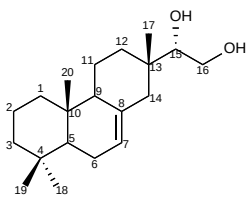

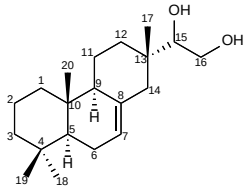

Esquirolin B

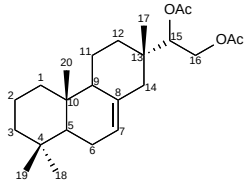

Esquirolin B

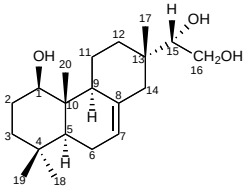

Ceriopsin C

[a]Chemical shifts from Li *et al.* (1991)
[b]Chemical shifts from Urones *et al.* (1998)
[C]Chemical shifts from Anjaneyulu and Rao (2002)

The ^{1}H and ^{13}C chemical shifts of Compound **2** were compared with those of the compound esquirolin B from the study of Li *et al.* (1991), which showed very similar values. This is also supported by the chemical shifts from the study of Urones *et al.* (1998), except for the chemical shifts of carbons and protons at positions 15, 16, and 17 due to the presence of acetate groups instead of hydroxyl groups. Although they did not specify assignments of the methyl protons to the respective carbons (C17–C20), the chemical shift values are in the same range (0.80–0.91) as those of Compound **2**, having only one methyl with a chemical shift of 0.91. The assignments of these methyl protons were in agreement with Anjaneyulu and Rao (2002) for the structure of ceriopsin C, which has a similar structure with Compound **2**, having only a hydroxyl group at C-1. Due to the presence of this hydroxyl group in ceriopsin C, the chemical shift of C-20 became more downfield, while H-20 became more upfield than the chemical shifts of Compound **2**.

Table IV. Comparison of ^{1}H and ^{13}C chemical shifts of (**3**) and betulinic acid.

	^{1}H chemical shift (δ_H) ($CDCl_3$, 400 MHz)	**^{1}H chemical shift (δ_H) ($CDCl_3$, 850.23 MHz)***	**^{13}C chemical shift (δ_C) ($CDCl_3$, 100 MHz)**	**^{13}C chemical shift (δ_C) ($CDCl_3$, 213.81 MHz)***
1	0.88, m; 1.67, m	0.912, td (13.4, 3.7 Hz); 1.678, dt (13.4, 3.7 Hz)	38.7	38.72
2	1.58, m	1.616, m; 1.564, m	27.4	27.43
3	3.20, dd (11.2, 4.8 Hz)	3.188, dd (11.7, 4.7 Hz)	79.0	79.01
4			38.9	38.8
5	0.67, br d (10.4 Hz)	0.685, d b (9.7 Hz)	55.3	55.37
6		1.523, m; 1.383, m	18.3	18.31
7	1.38, m	1.398, m; 1.370, m	34.3	34.43
8			40.7	40.67
9	1.26, m	1.273, t b	50.5	50.52
10			37.2	37.02
11	1.43, m	1.432 m; 1.270, t (13.2 Hz)	20.8	20.96
12	1.02, m	1.706, m; 1.039, ddd (28.7, 12.8, 4.7 Hz)	25.5	25.54
13	2.19, dt (12.0, 3.6 Hz)	2.199, ddd (13.8, 12.1, 3.8 Hz)	38.4	38.44
14			42.4	42.44
15	1.56, m; 1.22, m	1.982, m; 1.408, m	29.7	30.59
16	1.45, m; 2.26, m	2.271, dt (13.1, 3.4 Hz); 1.432, m	32.1	32.16
17			56.3	56.26
18	1.60, m	1.614, m	49.3	49.1
19	3.01, dt (10.8, 4.8 Hz)	3.001, dd (11.7, 4.6 Hz)	46.9	46.88
20			150.4	150.39
21	1.97, m	1.976, m; 1.483, m	37.0	37.01
22	1.40, m	1.521, m; 1.198, dt (3.7, 3.3 Hz)	30.5	29.72
23	0.962, s	0.967, s	27.9	27.99
24	0.75, s	0.756, s	15.3	15.35
25	0.821, s	0.939, s	16.1	16.03
26	0.933, s	0.827, d b	16.0	16.14
27	0.972, s	0.977, d (0.8 Hz)	14.7	14.71
28			180.1	179.37
29	4.60, br dd (2.0, 1.6 Hz); 4.73, br d (2.0 Hz)	4.743, m; 4.610, m	109.7	109.73
30	1.687, s	1.693, td b	19.4	19.38

*^{1}H and ^{13}C chemical shifts from Dais *et al*. (2017)

^{1}H chemical shift differences can be due to differences in concentration, temperature, and sometimes pH (CDCl3). To establish the identity of the compound, ^{13}C-NMR shifts are better references.

Table V. Comparison of ^{1}H and ^{13}C chemical shifts of (**4**) and lupeol.

	^{1}H chemical shift (δ_H) ($CDCl_3$, 400 MHz)	**^{1}H chemical shift (δ_H) ($CDCl_3$, 400 MHz)***	**^{13}C chemical shift (δ_C) ($CDCl_3$, 100 MHz)**	**^{13}C chemical shift (δ_C) ($CDCl_3$, 100 MHz)***
1	0.89, m		38.8	38.8
2	1.58, m	1.89, m	27.4	27.5
3	3.21, t (4.8 Hz)	3.16, m	79.0	79.0
4			38.9	38.9
5	0.68, m	0.66, m	55.3	55.3
6	1.52, m	1.36, m	18.3	18.9
7	1.38, m		34.3	34.3
8			40.8	40.8
9	1.26, m	1.24, s	50.4	50.4
10			37.2	37.2
11	1.11, m		20.9	21.0
12	1.05, m; 1.23, m		25.1	25.1
13	1.63, m		38.0	38.1
14			42.8	42.1
15	1.69, m		27.4	27.4
16	1.48, m; 1.35, m		35.6	35.6
17			43.0	43.1
18	1.36, m		48.3	48.3
19	2.38, dt (1.2, 6 Hz)	2.37, m	48.0	48.0
20			151	150.9
21	1.93, m		29.8	29.9
22	1.40, m		40.0	40.1
23	0.97, s	0.94, s	28.0	28.1
24	0.76, s	0.74, s	15.4	15.5
25	0.83, s	0.8, s	16.1	16.0
26	1.03, s	1.01, s	16.0	16.2
27	0.94, s	0.92, s	14.5	14.6
28	0.79, s	0.77, s	18.0	18.1
29	4.56, br dd (2.4, 1.2 Hz); 4.68, br d, (2.8 Hz)	4.67, s; 4.55, s	109.3	109.5
30	1.68, s	1.66, s	19.3	19.4

*^{1}H and ^{13}C chemical shifts from Beserra *et al*. (2018)

^{1}H chemical shift differences can be due to differences in concentration, temperature, and sometimes pH (CDCl3). To establish the identity of the compound, ^{13}C-NMR shifts are better references.

Table VI. Comparison of ^{1}H and ^{13}C chemical shifts of (**5**) and methyl 6-methyl-2,4-dihydroxybenzoate.

	^{1}H chemical shift (δ_H) ($CDCl_3$, 400 MHz)	**^{1}H chemical shift (δ_H)* ($CDCl_3$, 400 MHz)**	**^{13}C chemical shift (δ_C) ($CDCl_3$, 100 MHz)**	**^{13}C chemical shift (δ_C)* ($CDCl_3$, 100 MHz)**
1			105.7	104.5
2			165.3	165.3
3	6.28, d (2.8 Hz)	6.28, s	101.2	100.9
4			160.2	160.3
5	6.22, dd (2.4, 0.8 Hz)	6.23, s	111.3	111.3
6			144.0	144.0
7			172.1	172.1
8	2.49, s	2.49, s	24.3	24.2
9	3.92, s	3.92, s	51.9	51.9
	11.74, s, 2-OH	11.75, s, OH		
	5.36, s, 4-OH			

*^{1}H and ^{13}C chemical shifts from Basset *et al*. (2010)

APPENDIX III

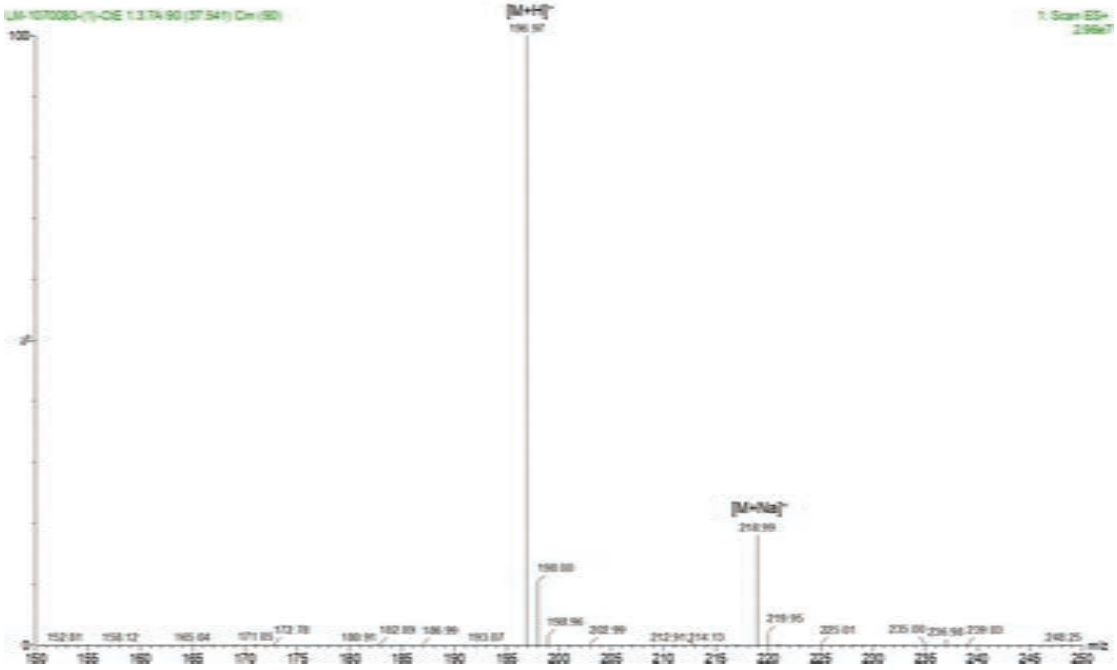

Figure I. ESI-MS spectrum of CtE 1.3.7A (**1**)

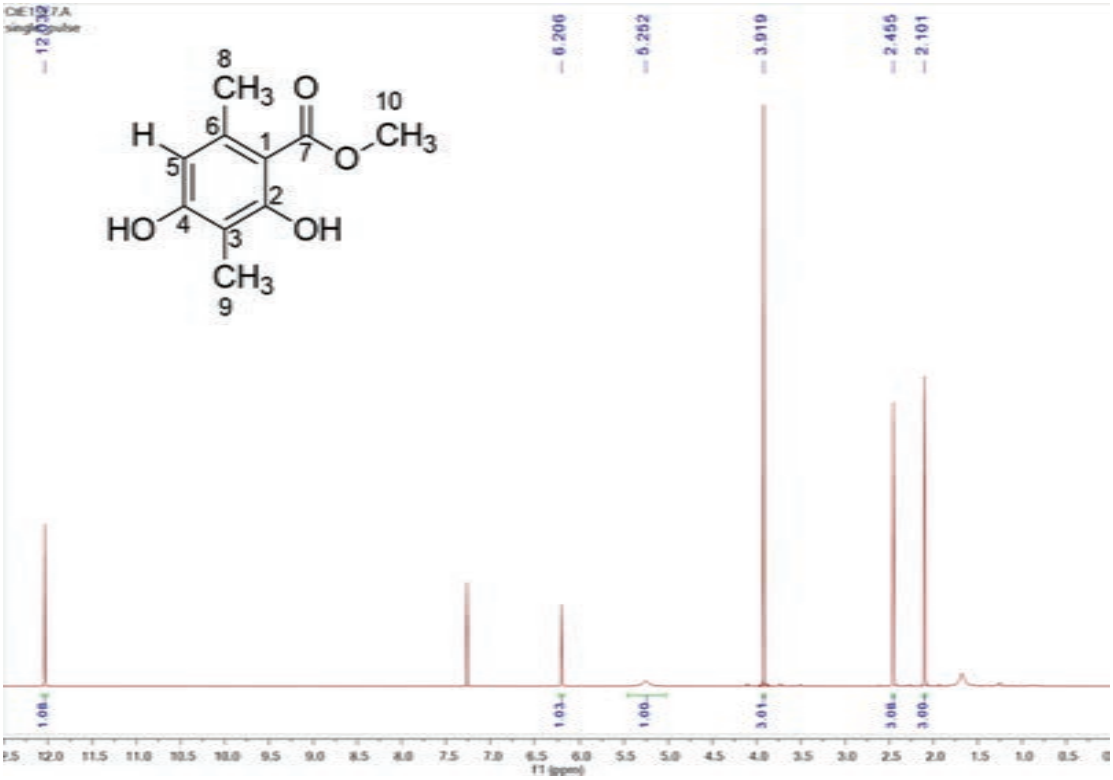

Figure II. ^{1}H NMR spectrum of CtE 1.3.7A (**1**) in $CDCl_3$, 400 MHz

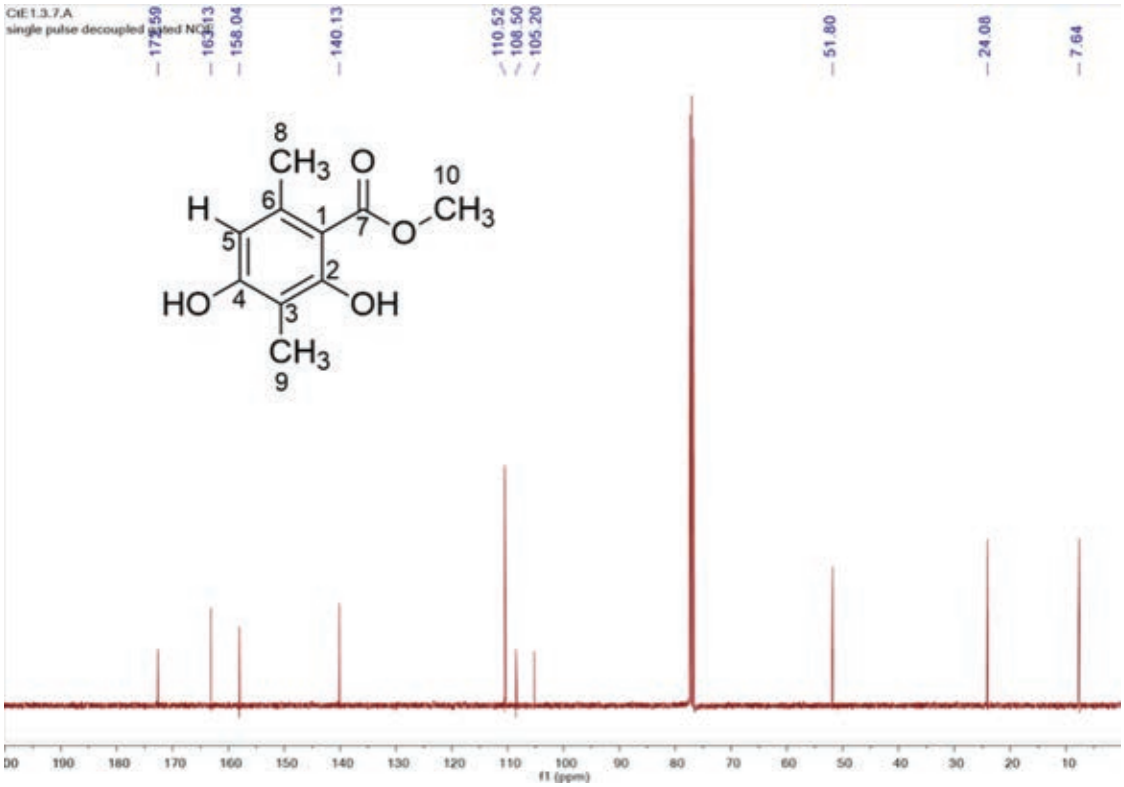

Figure III. ^{13}C NMR spectrum of CtE 1.3.7A (**1**) in $CDCl_3$, 100 MHz

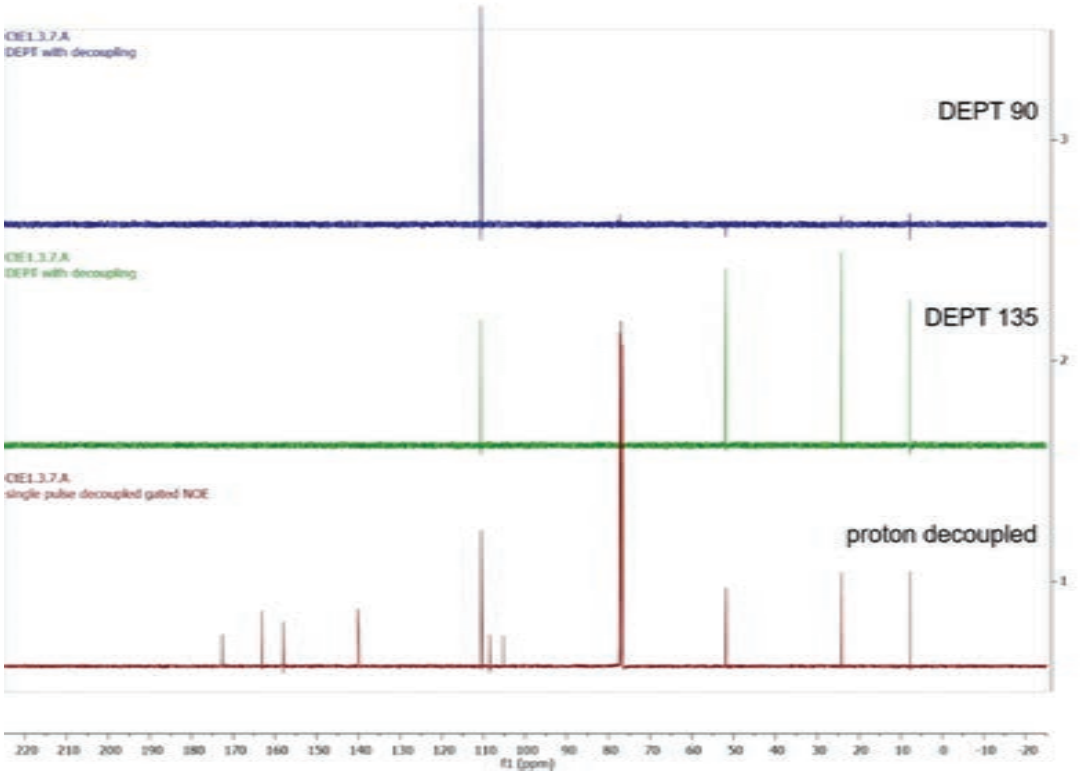

Figure IV. DEPT ^{13}C NMR spectrum of CtE 1.3.7A (**1**)

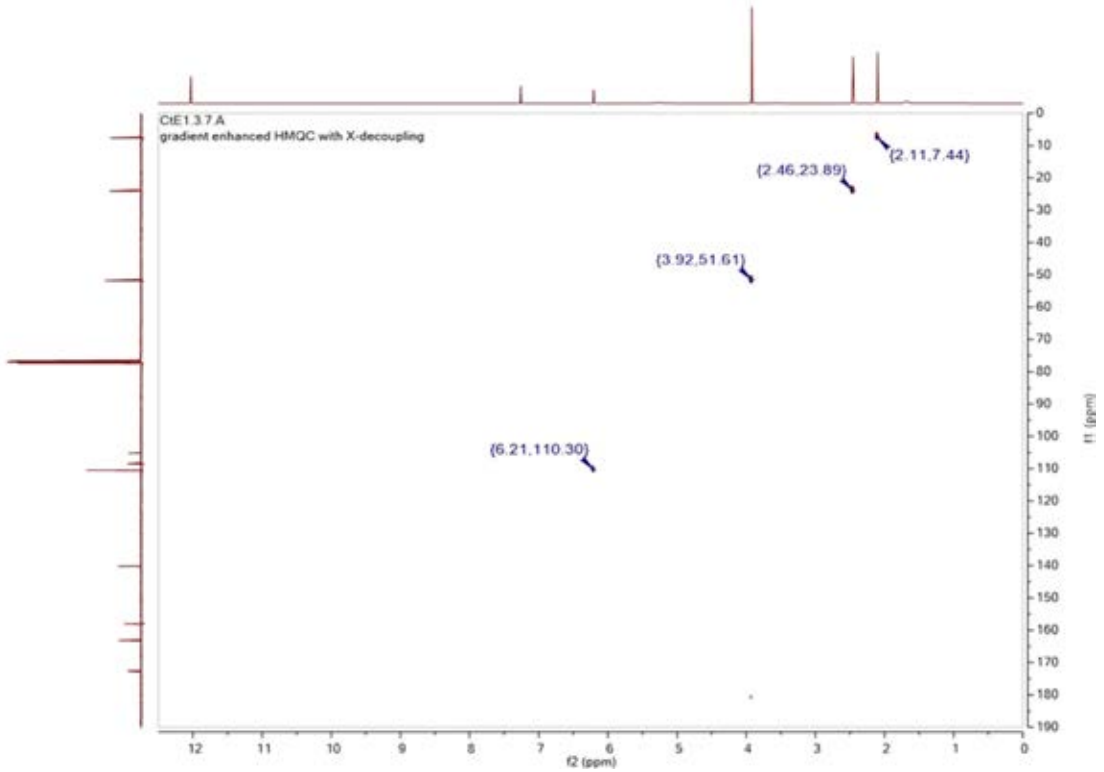

Figure V. HMQC spectrum of CtE 1.3.7A (**1**)

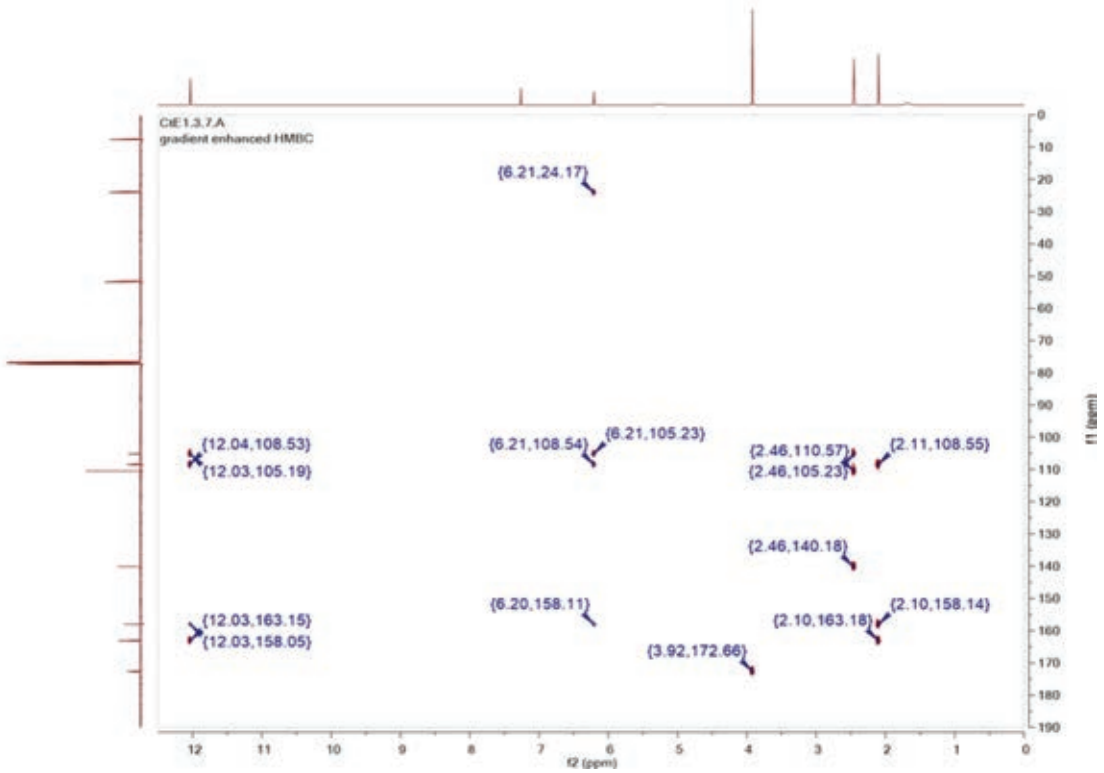

Figure VI. HMBC spectrum of CtE 1.3.7A (**1**)

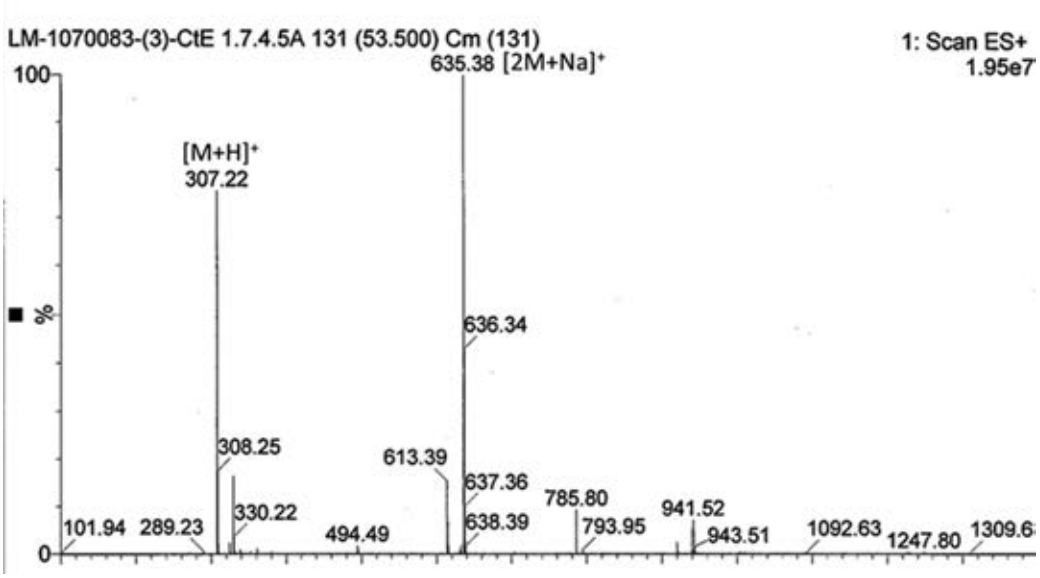

Figure VII. ESI-MS spectrum of CtE 1.7.4.5A (**2**)

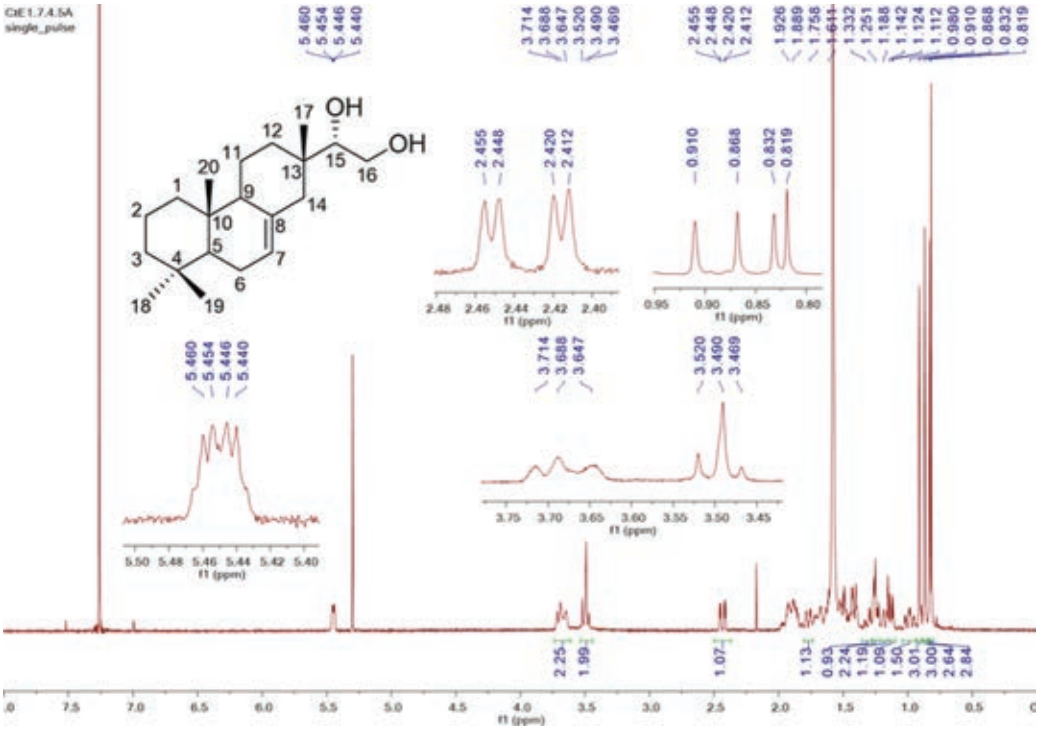

Figure VIII. ^{1}H NMR spectrum of CtE 1.7.4.5A (**2**) in $CDCl_3$, 400 MHz

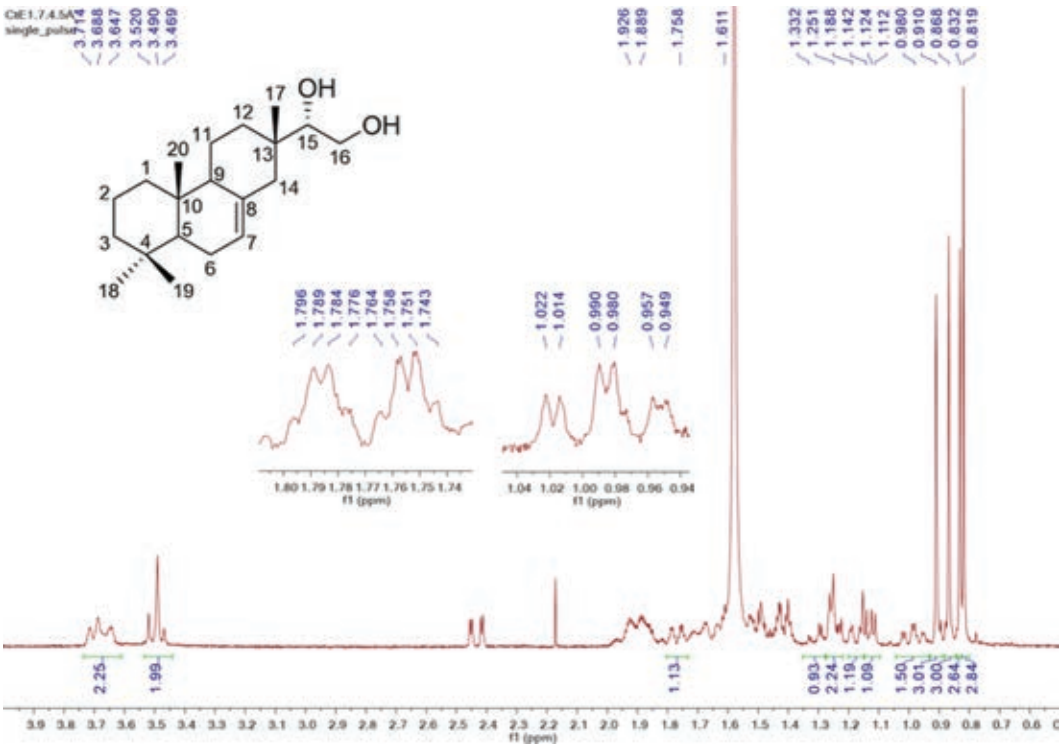

Figure IX. ^{1}H NMR spectrum of CtE 1.7.4.5A (**2**) in $CDCl_3$, 400 MHz (expansion)

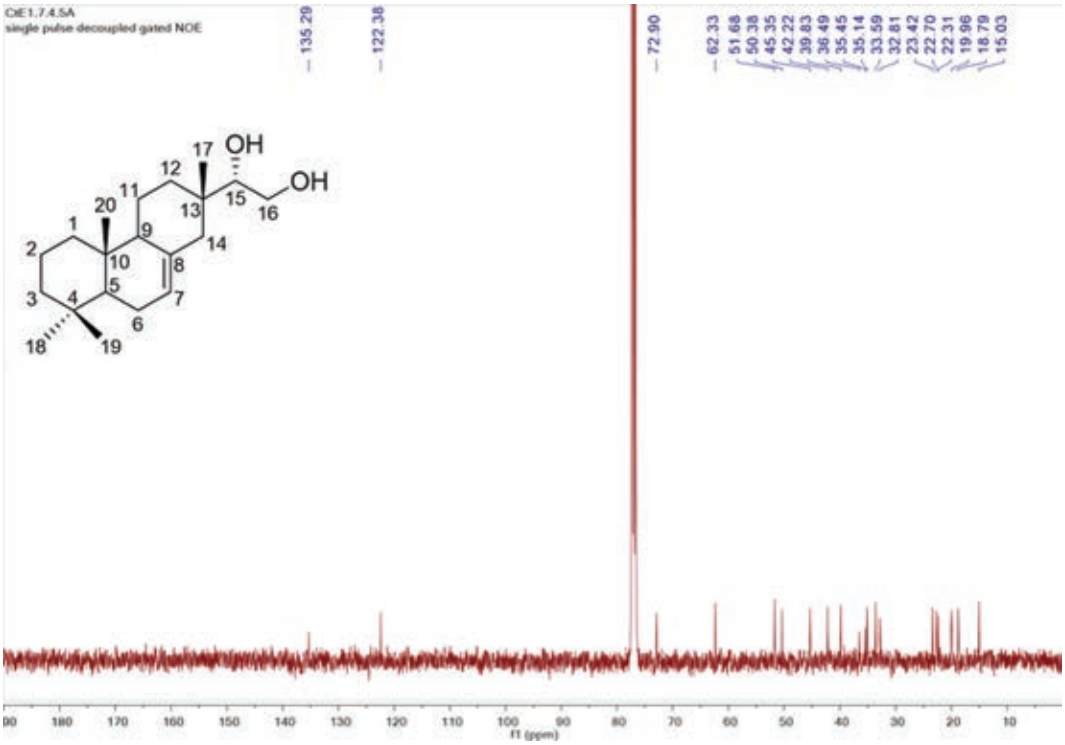

Figure X. ^{13}C NMR spectrum of CtE 1.7.4.5A (**2**) in $CDCl_3$, 100 MHz

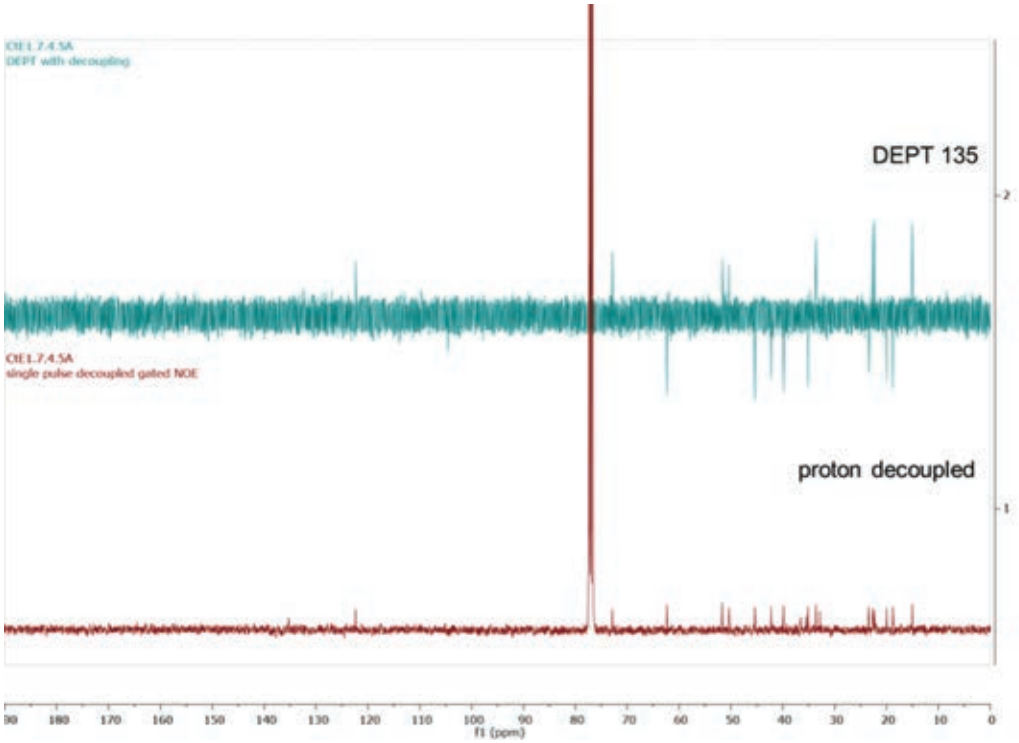

Figure XI. DEPT ^{13}C NMR spectrum of CtE 1.7.4.5A (**2**)

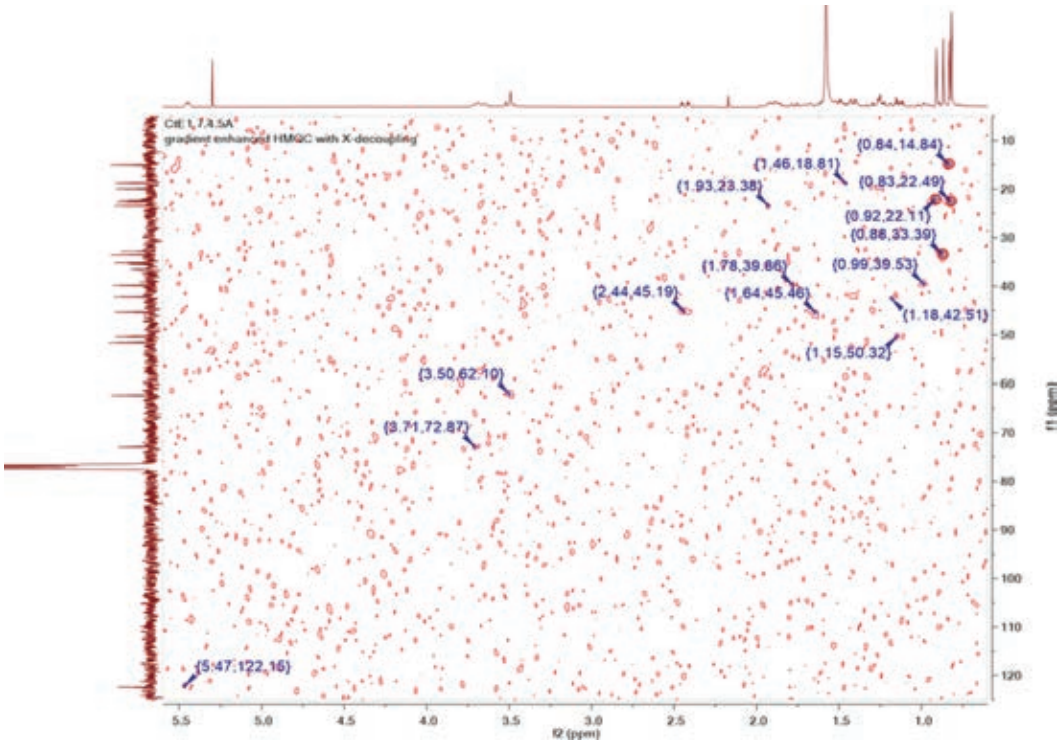

Figure XII. HMQC spectrum of CtE 1.7.4.5A (**2**)

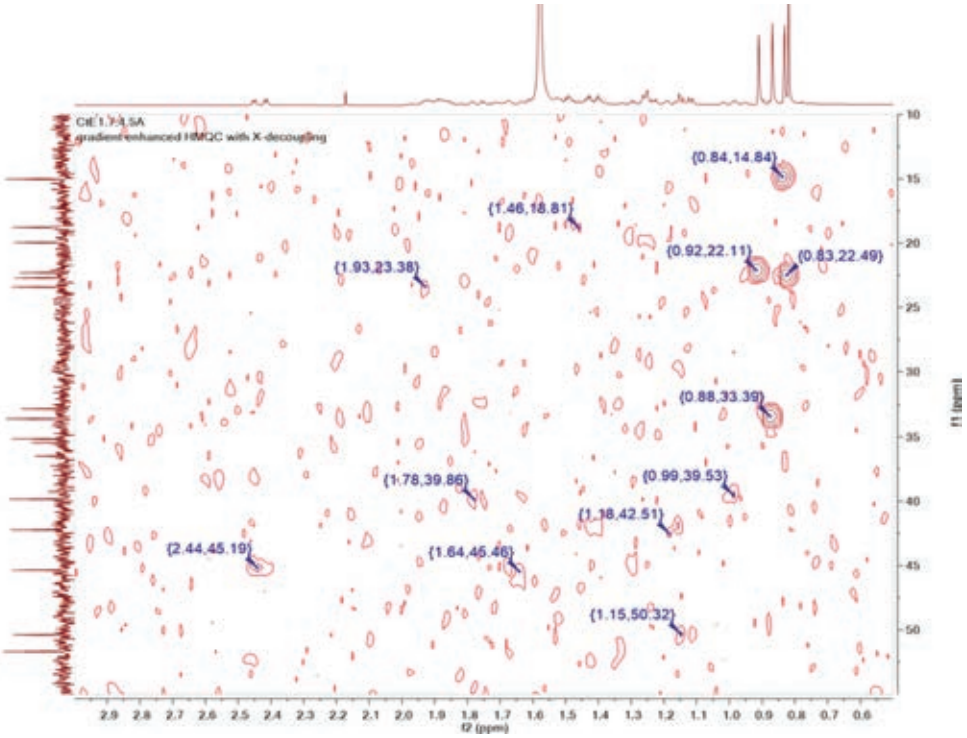

Figure XIII. HMQC spectrum of CtE 1.7.4.5A (**2**) (expansion)

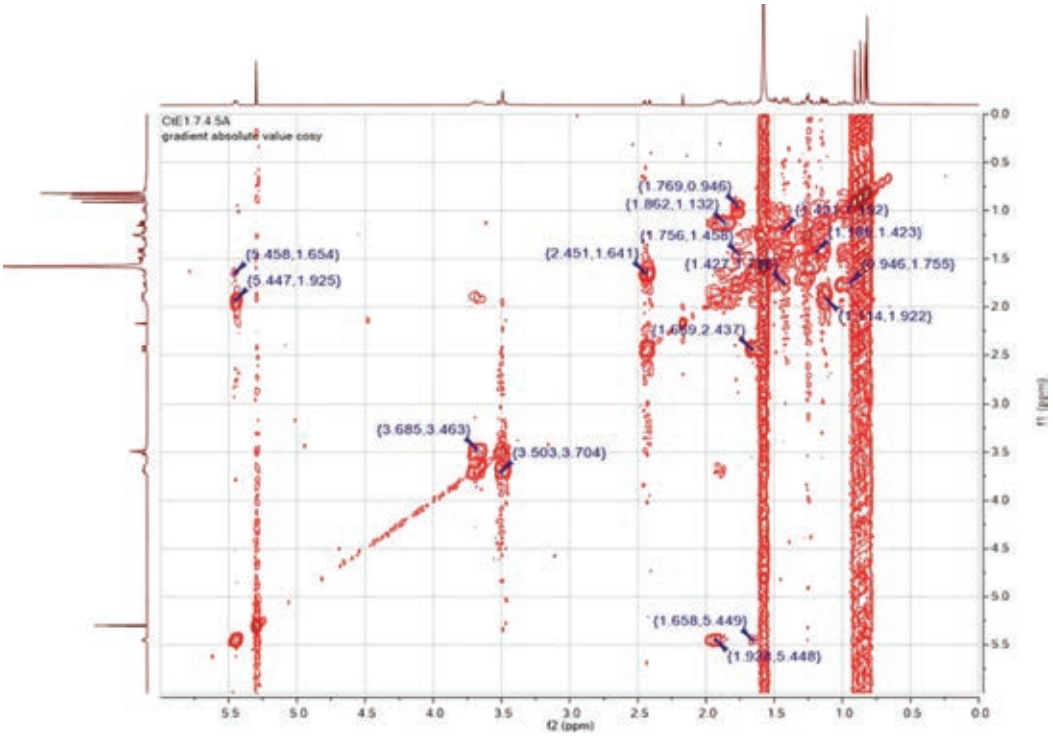

Figure XIV. COSY spectrum of CtE 1.7.4.5A (**2**)

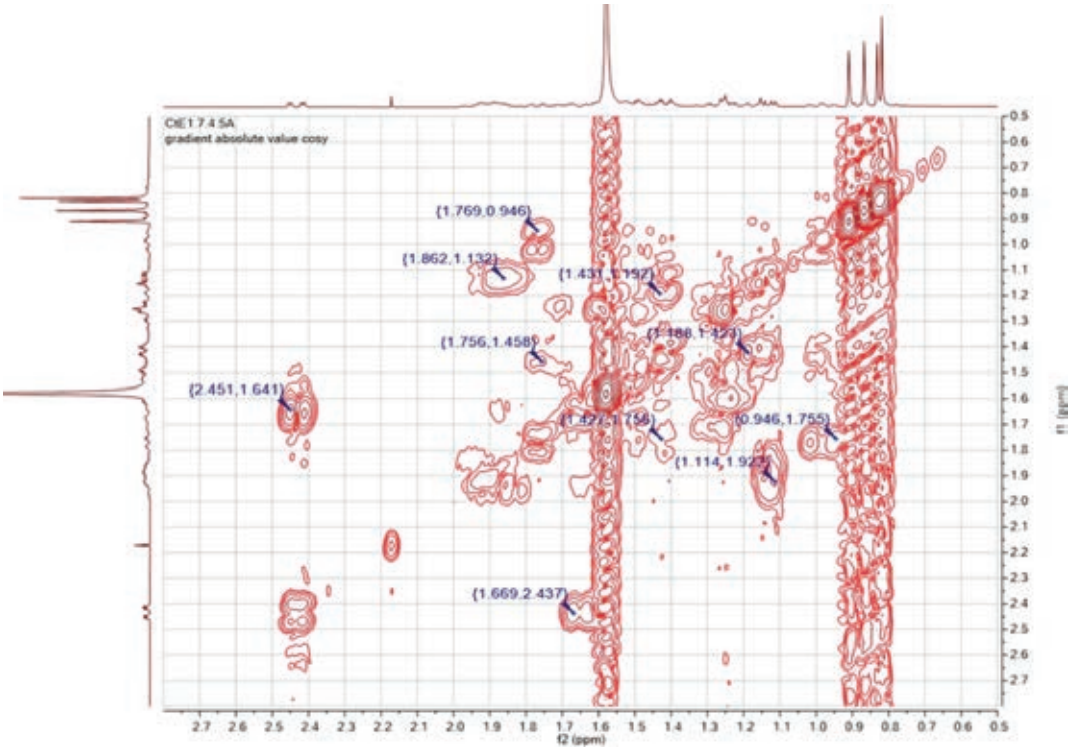

Figure XV. COSY spectrum of CtE 1.7.4.5A (**2**) (expansion)

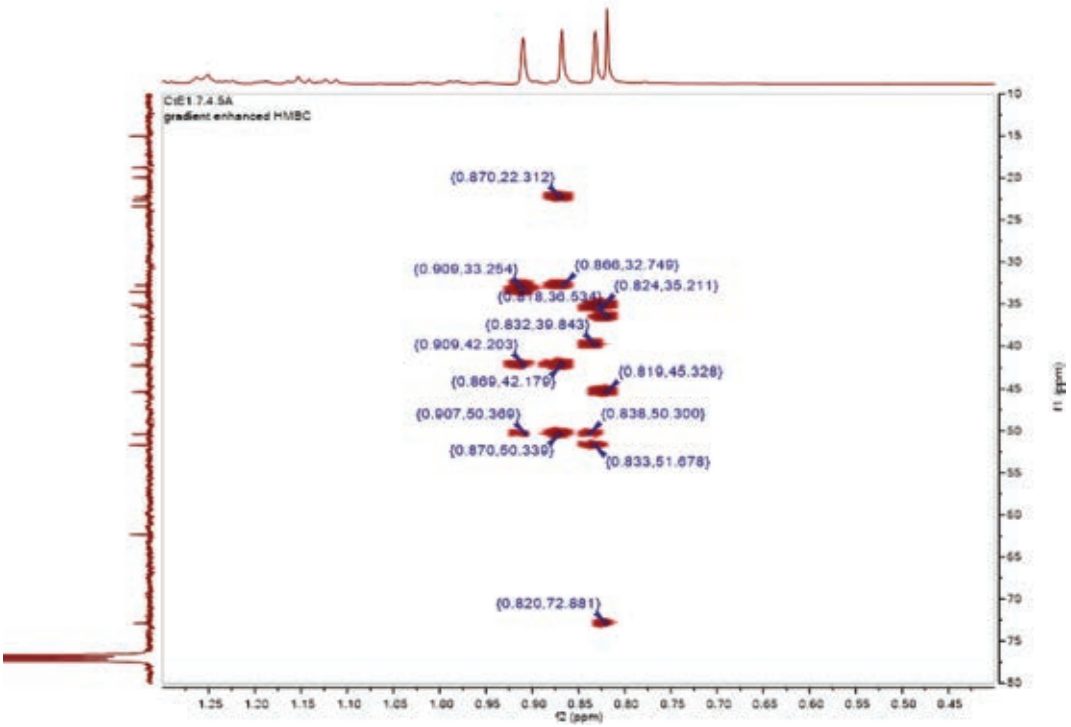

Figure XVI. HMBC spectrum of CtE 1.7.4.5A (**2**)

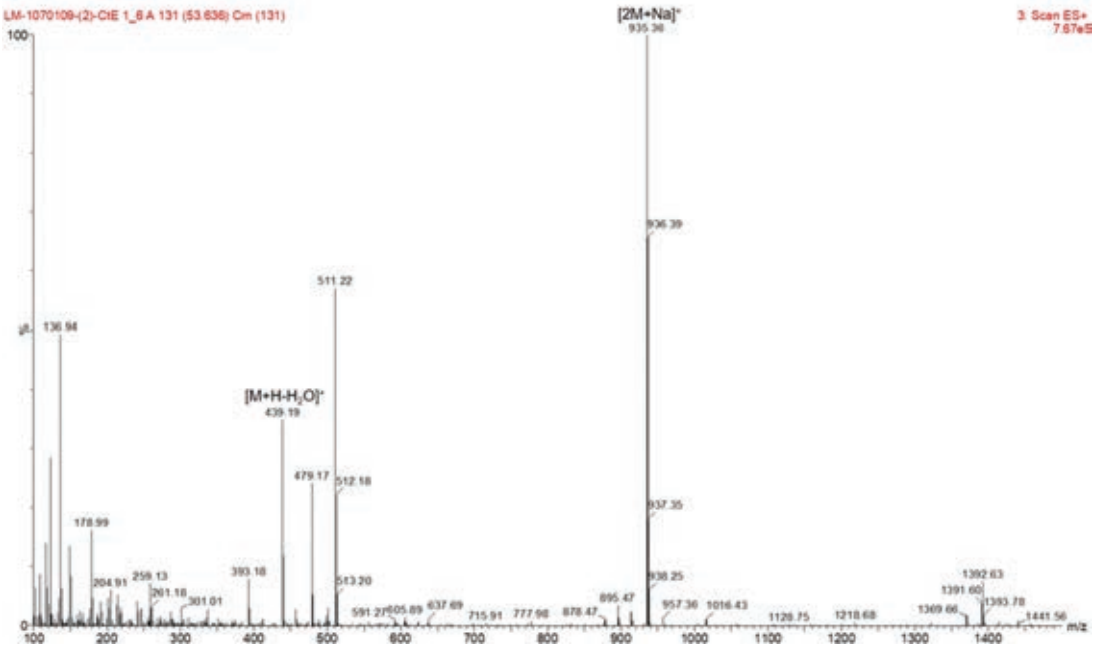

Figure XVII. ESI-MS spectrum of CtE 1.6A (**3**)

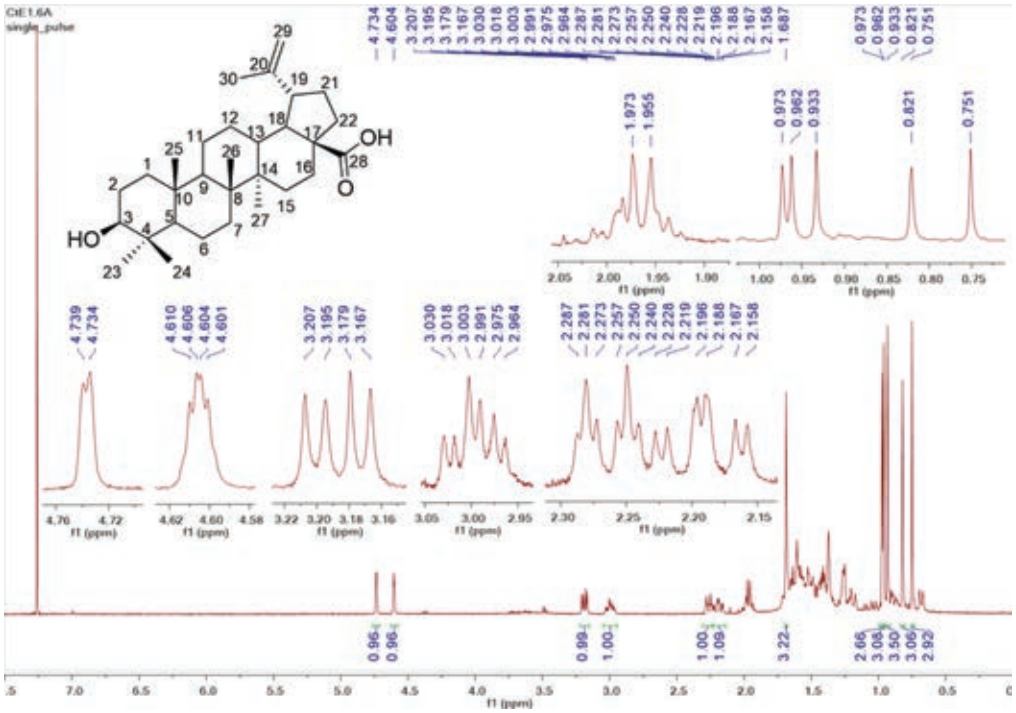

Figure XVIII. ^{1}H NMR spectrum of CtE 1.6A (**3**) in $CDCl_3$, 400 MHz

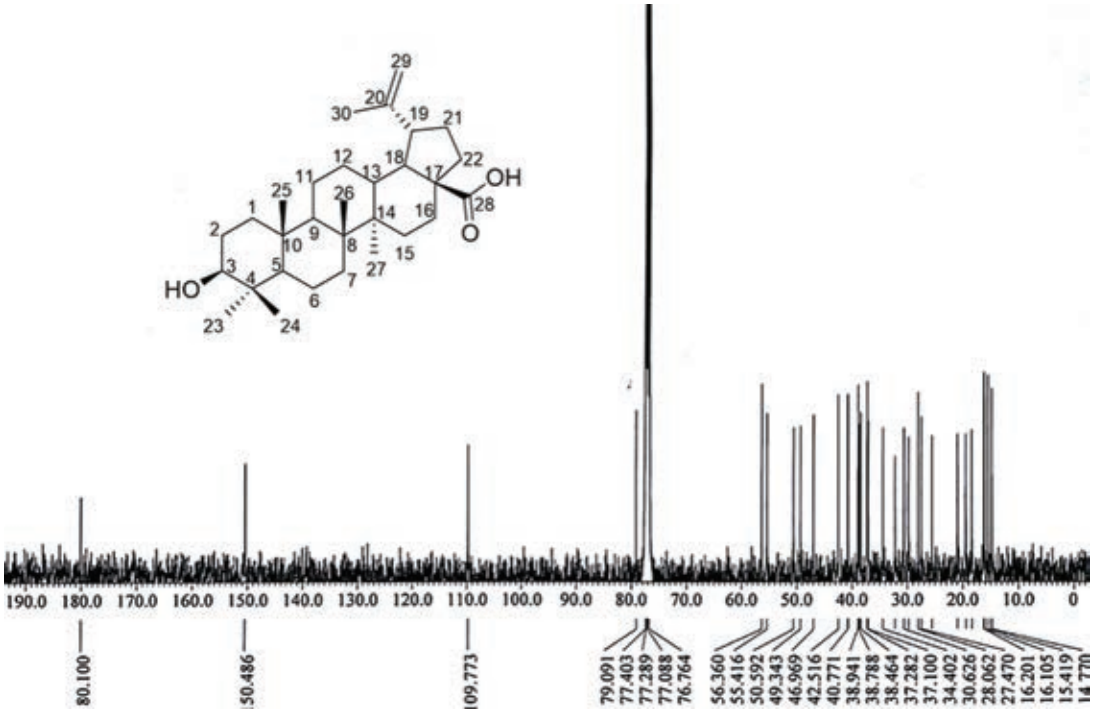

Figure XIX. ^{13}C NMR spectrum of CtE 1.6A (**3**) in $CDCl_3$, 100 MHz

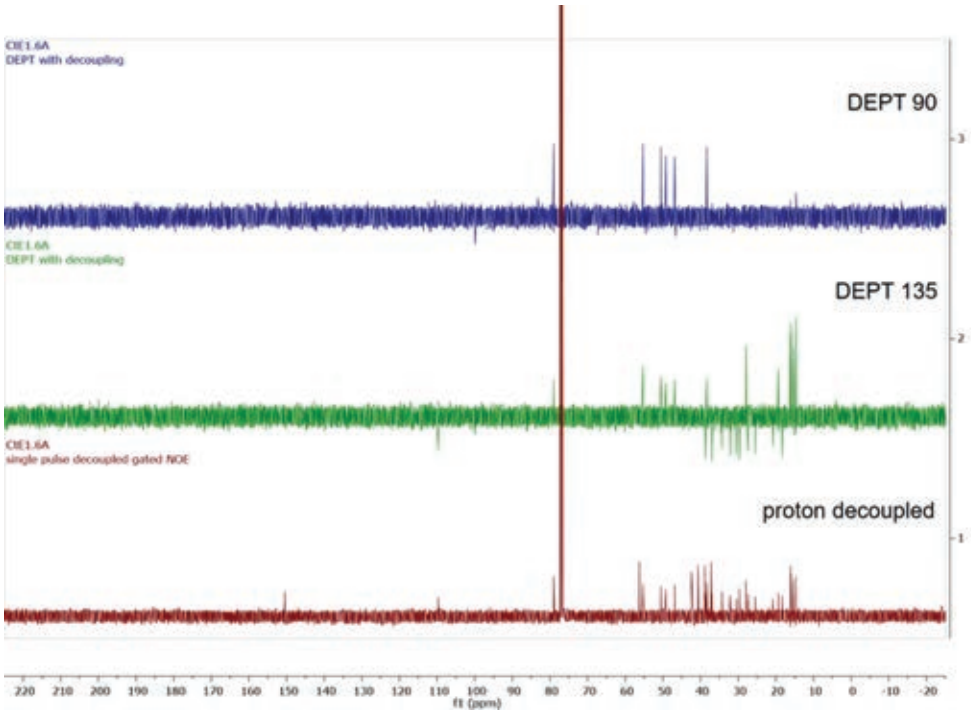

Figure XX. DEPT ^{13}C NMR spectrum of CtE 1.6A (**3**)

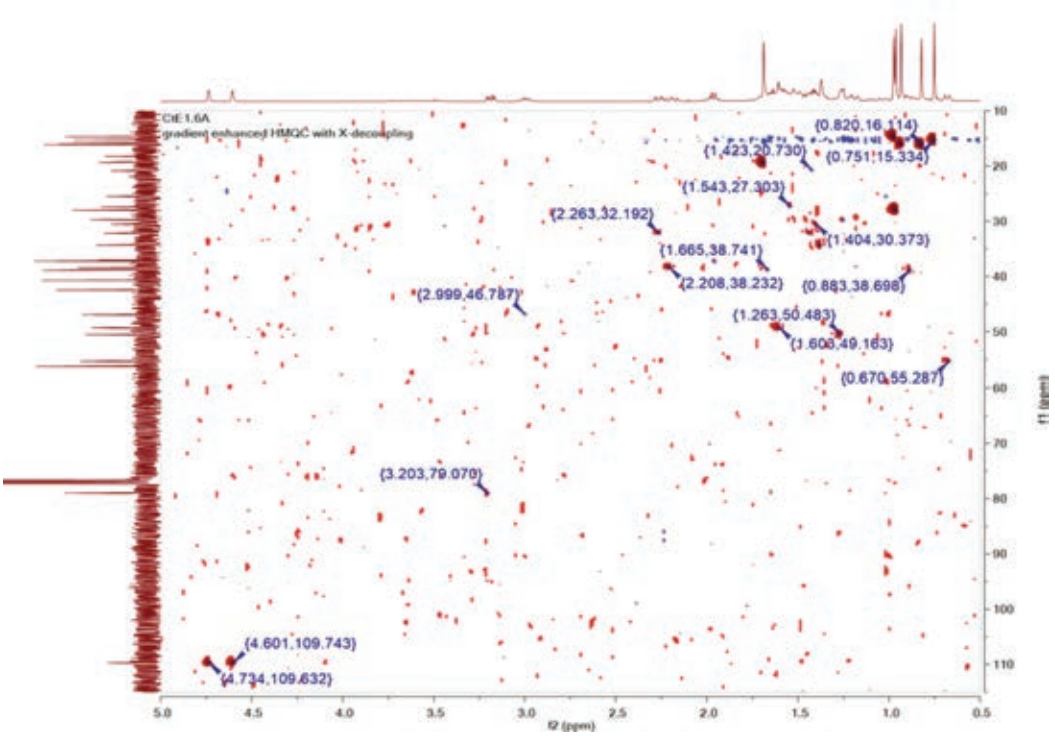

Figure XXI. HMQC spectrum of CtE 1.6A (**3**)

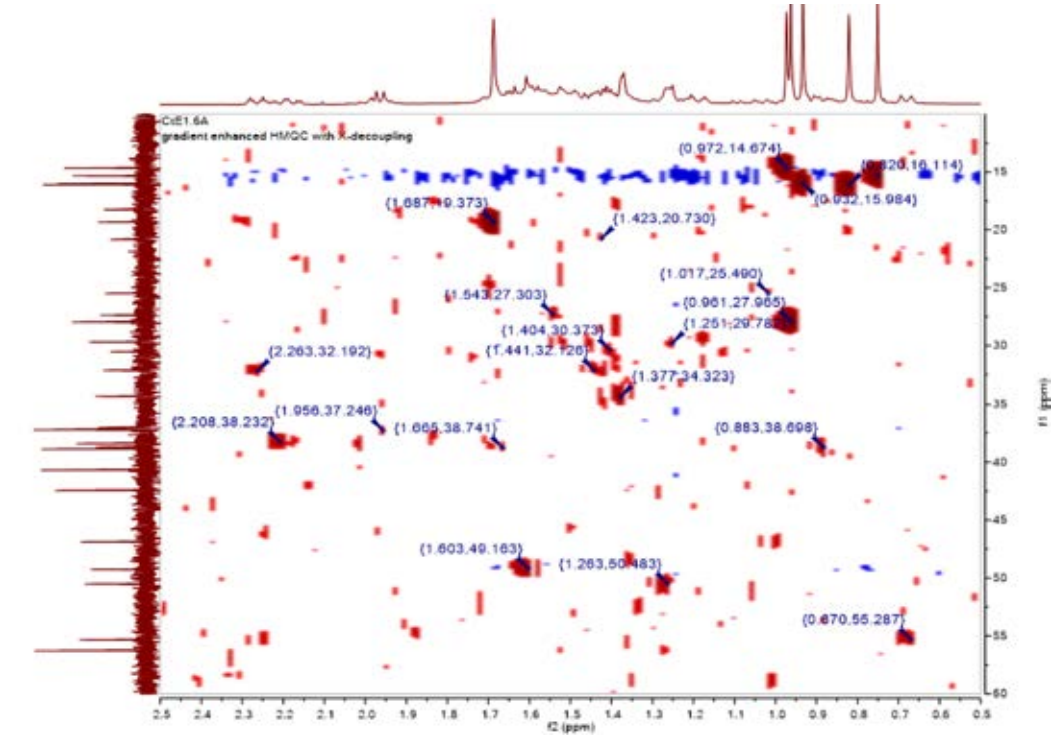

Figure XXII. HMQC spectrum of CtE 1.6A (**3**) (expansion)

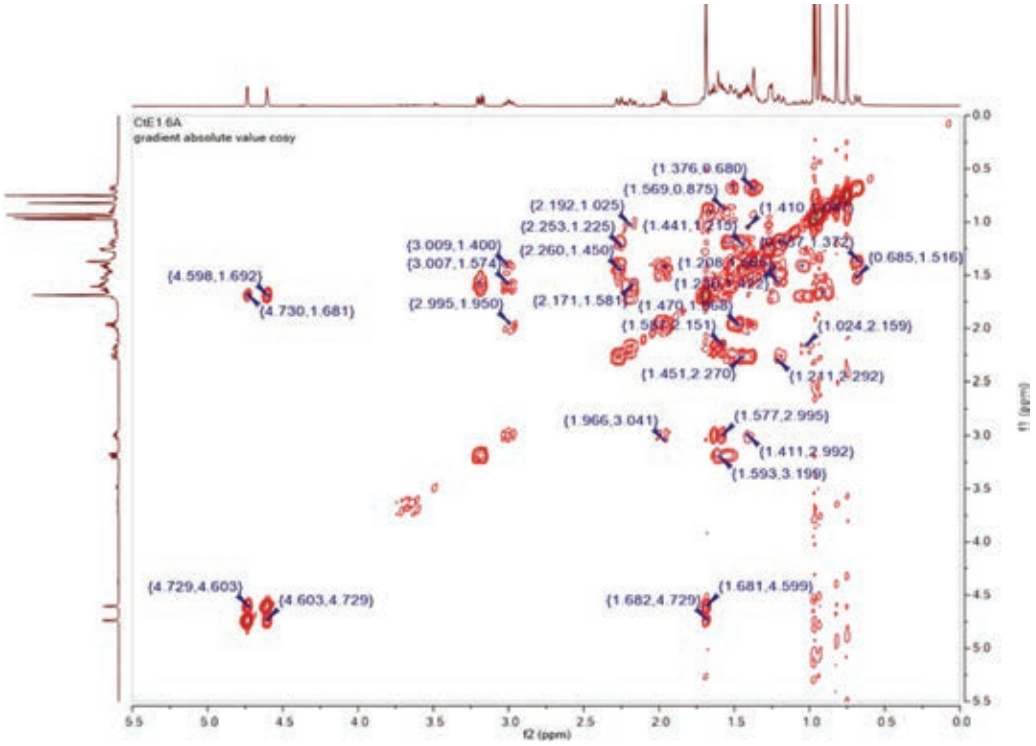

Figure XXIII. COSY spectrum of CtE 1.6A (**3**)

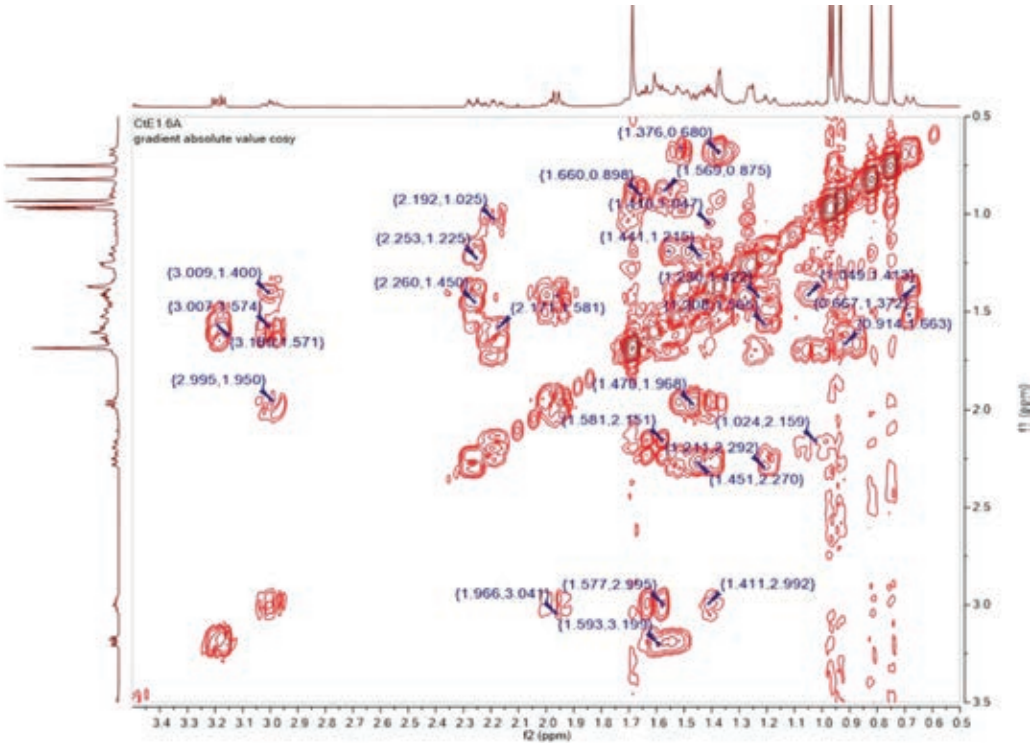

Figure XXIV. COSY spectrum of CtE 1.6A (**3**) (expansion 1)

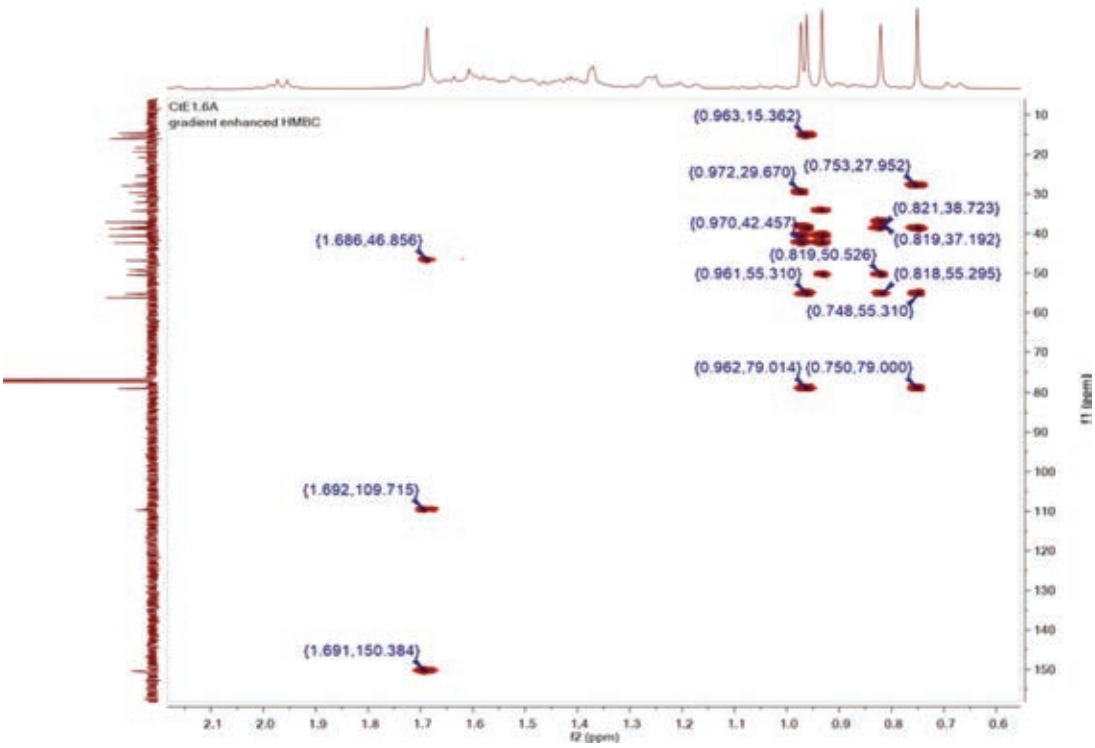

Figure XXV. HMBC spectrum of CtE 1.6A (**3**)

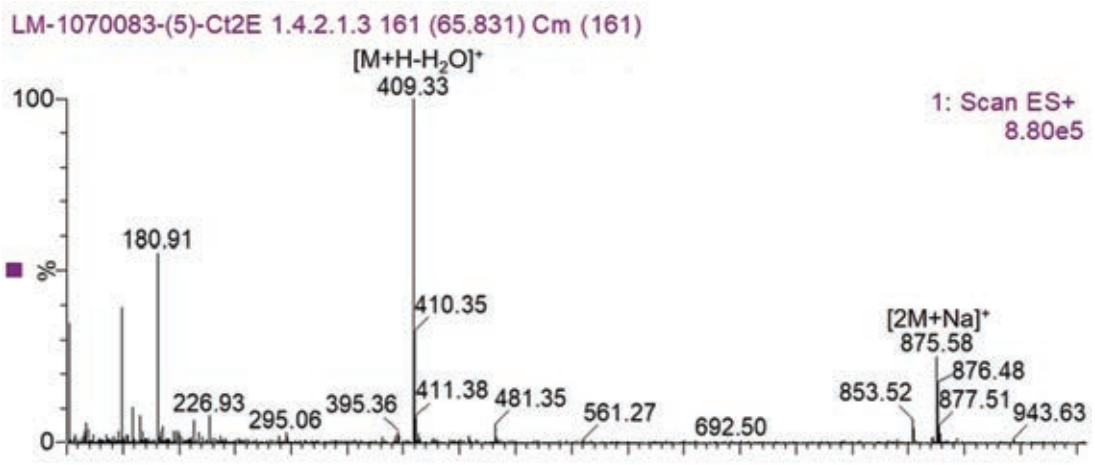

Figure XXVI. ESI-MS spectrum of Ct2E 1.4.2.1.3 (**4**)

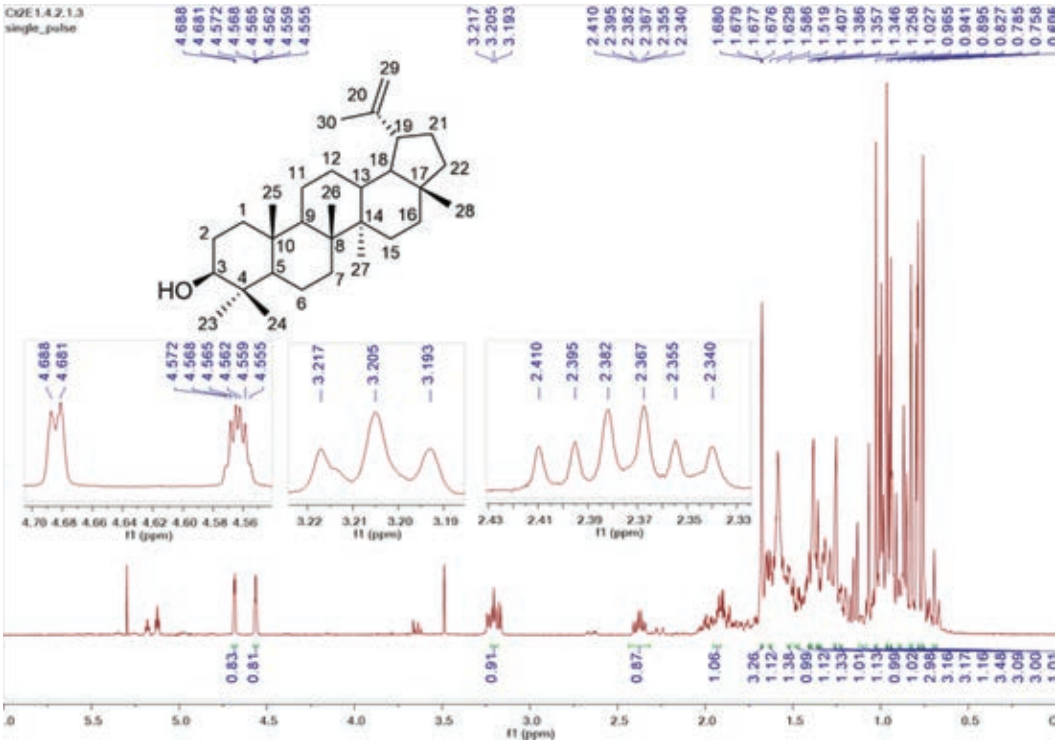

Figure XXVII. ^{1}H NMR Spectrum of Ct2E 1.4.2.1.3 (**4**) in $CDCl_3$, 400 MHz

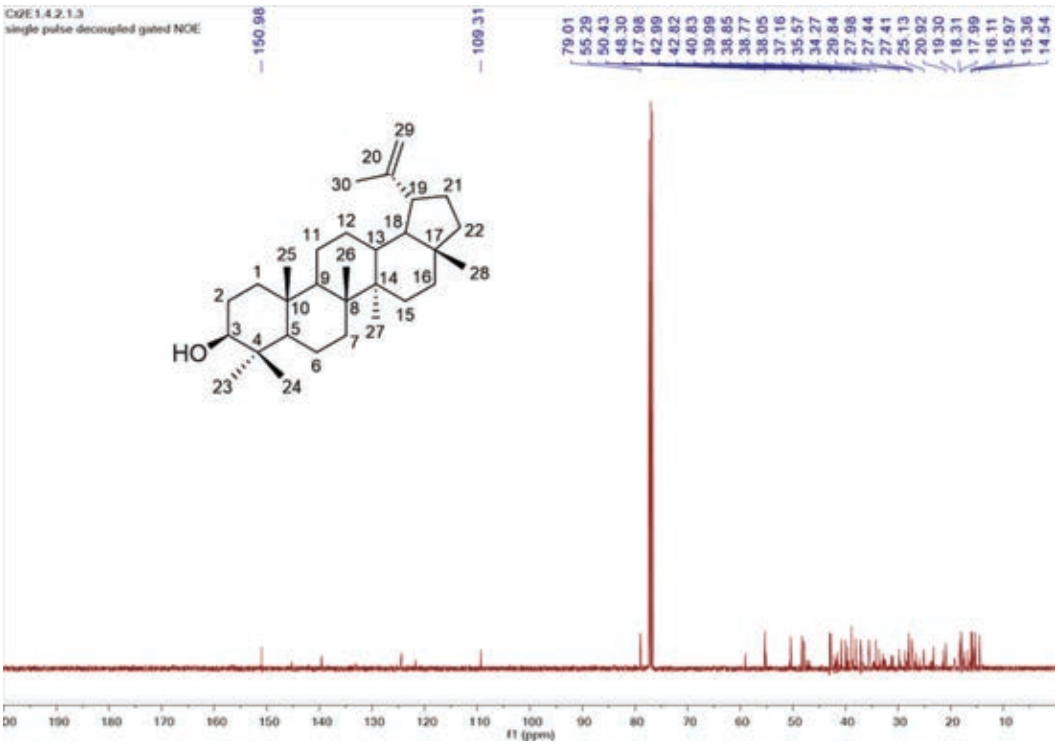

Figure XXVIII. ^{13}C NMR spectrum of Ct2E 1.4.2.1.3 (**4**) in $CDCl_3$, 100 MHz

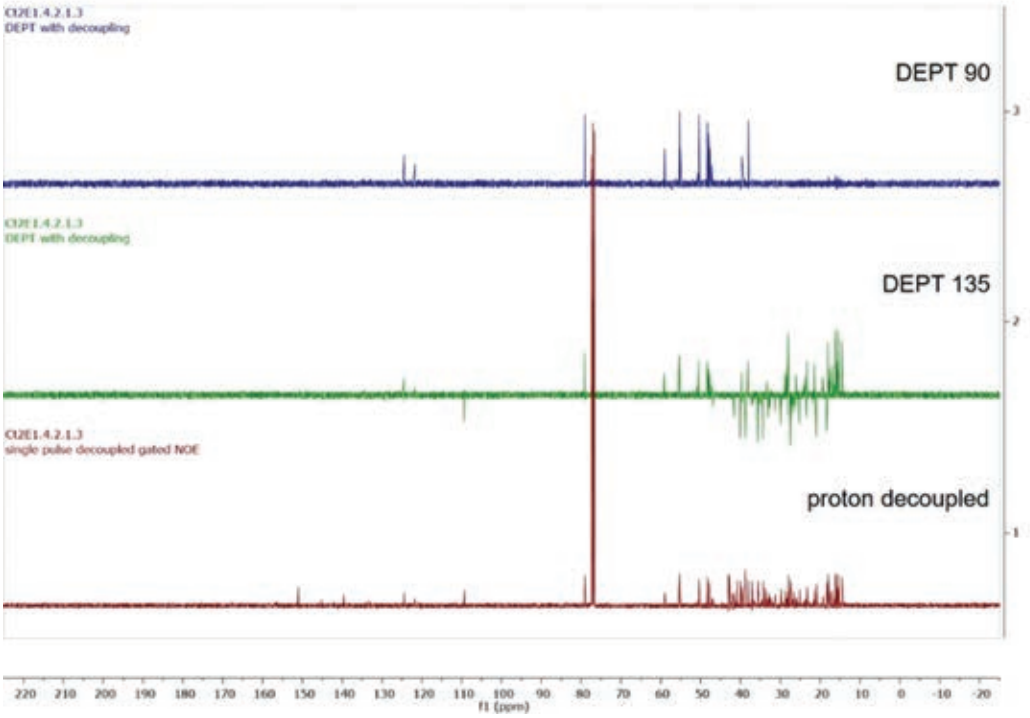

Figure XXIX. DEPT ^{13}C NMR spectrum of Ct2E 1.4.2.1.3 (**4**)

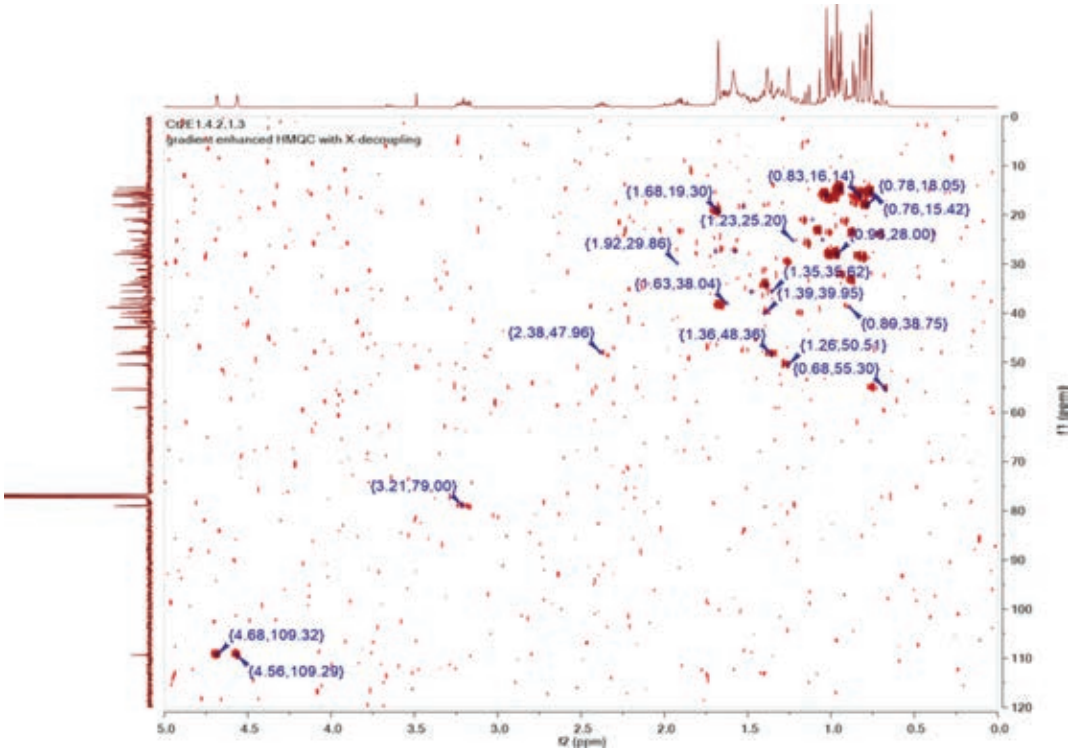

Figure XXX. HMQC spectrum of Ct2E 1.4.2.1.3 (**4**)

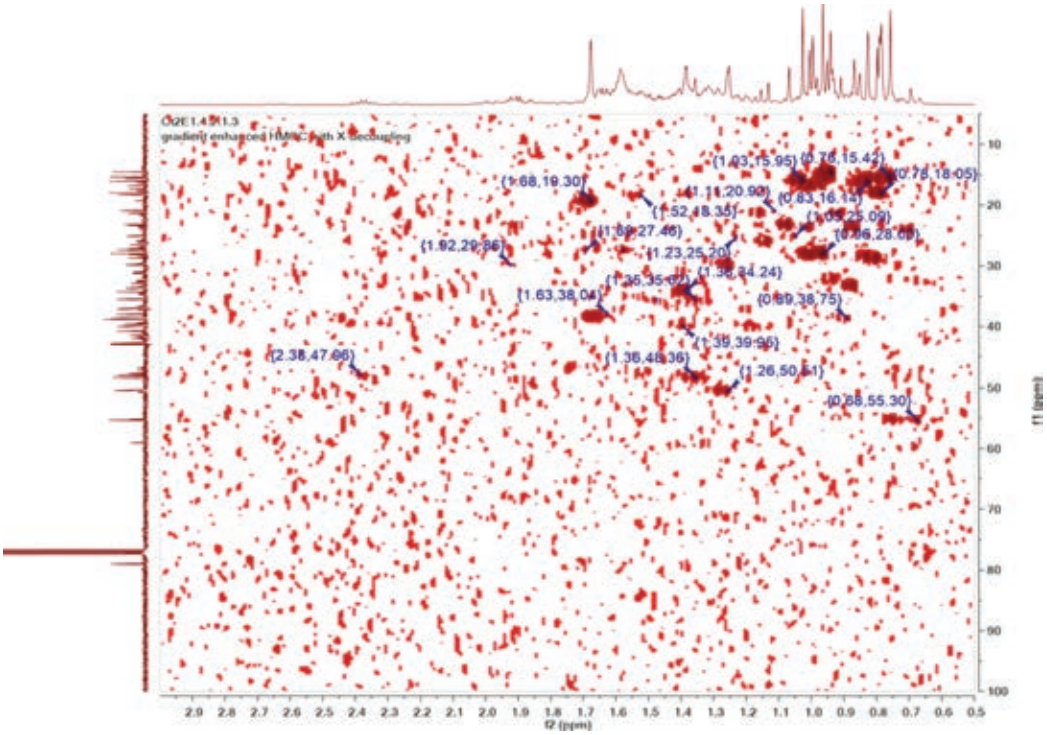

Figure XXXI. HMQC spectrum of Ct2E 1.4.2.1.3 (**4**) (expansion)

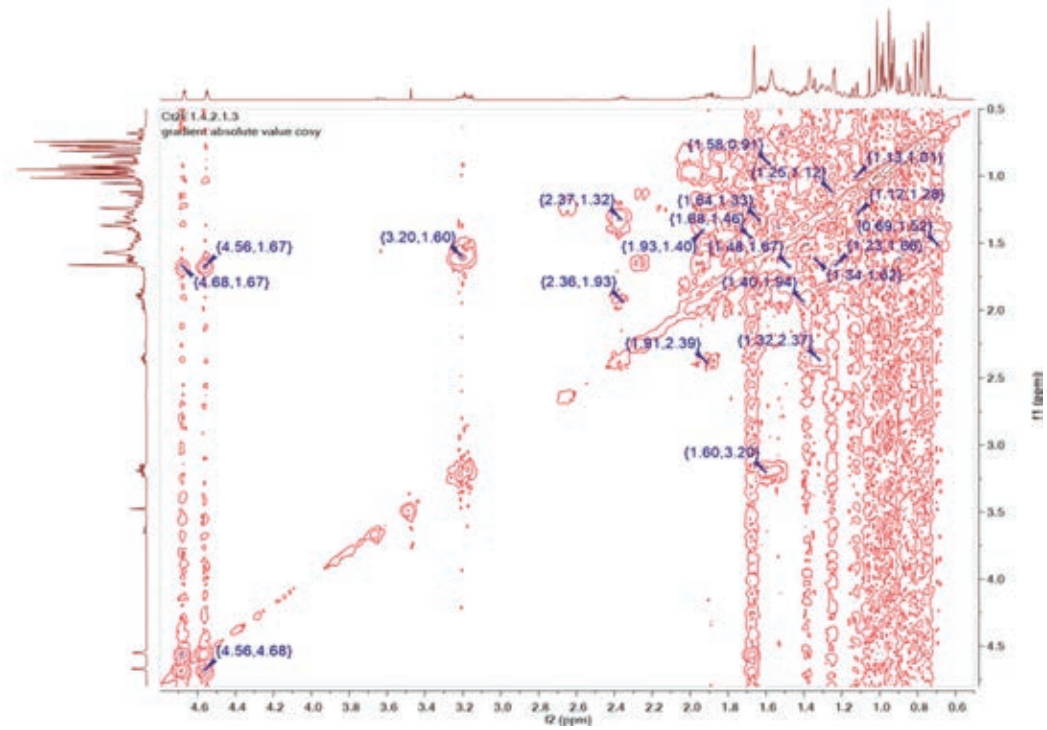

Figure XXXII. COSY spectrum of Ct2E 1.4.2.1.3 (**4**)

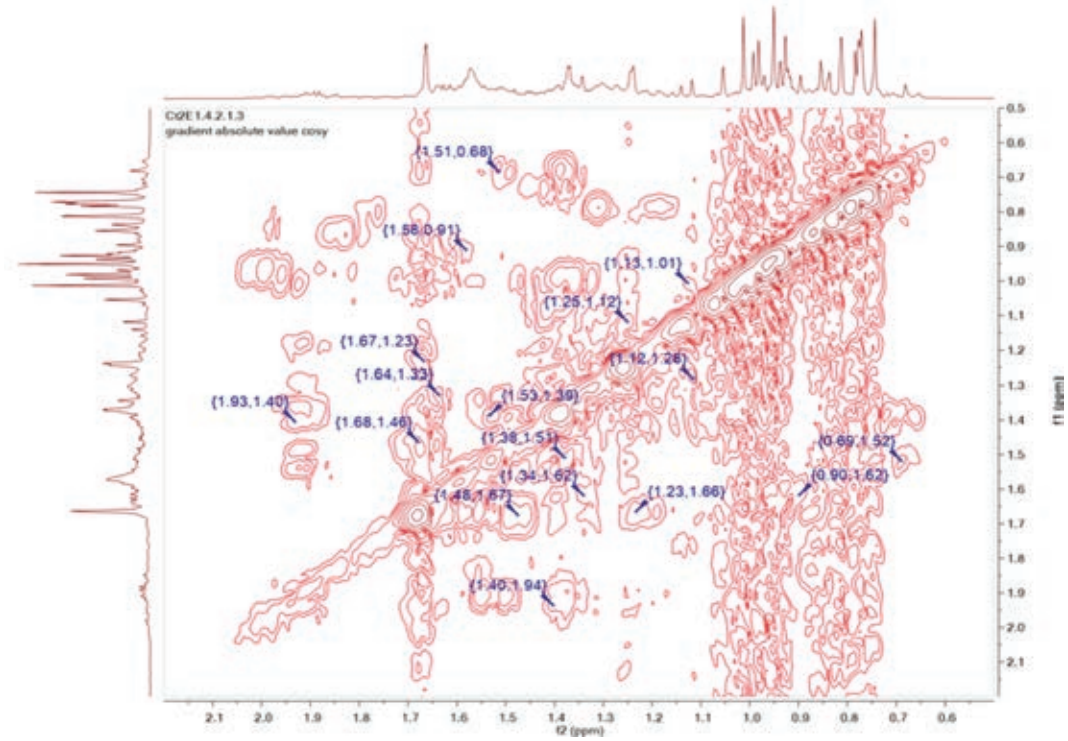

Figure XXXIII. COSY spectrum of Ct2E 1.4.2.1.3 (**4**) (expansion)

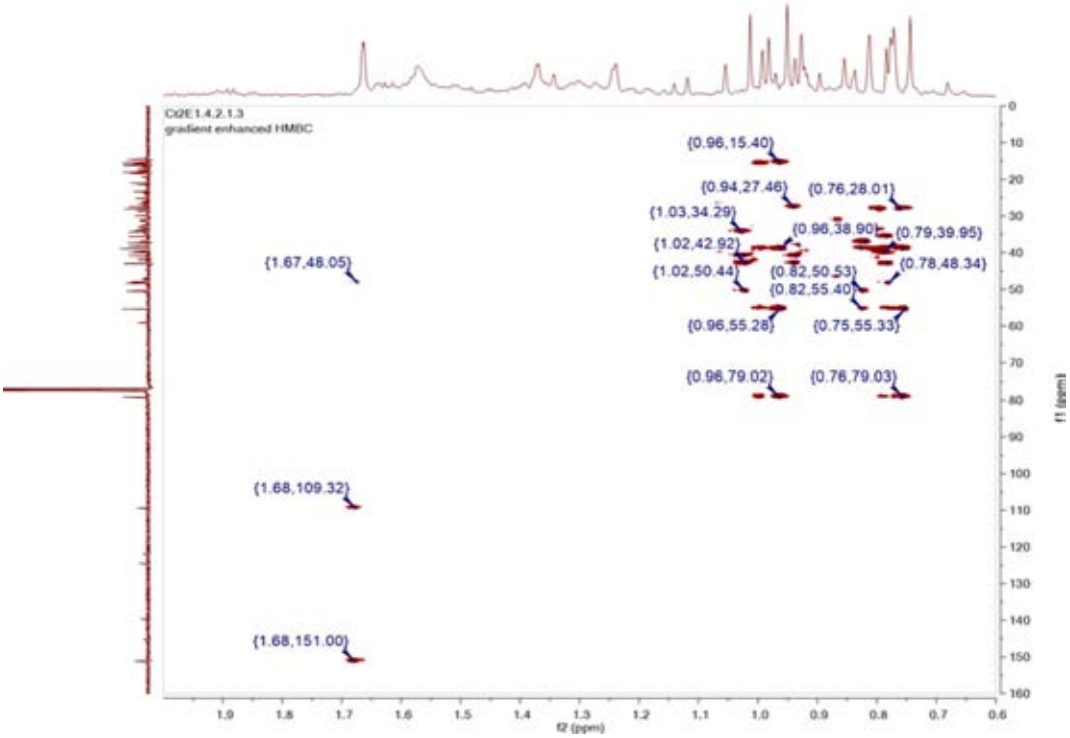

Figure XXXIV. HMBC spectrum of C2E 1.4.2.1.3 (**4**)

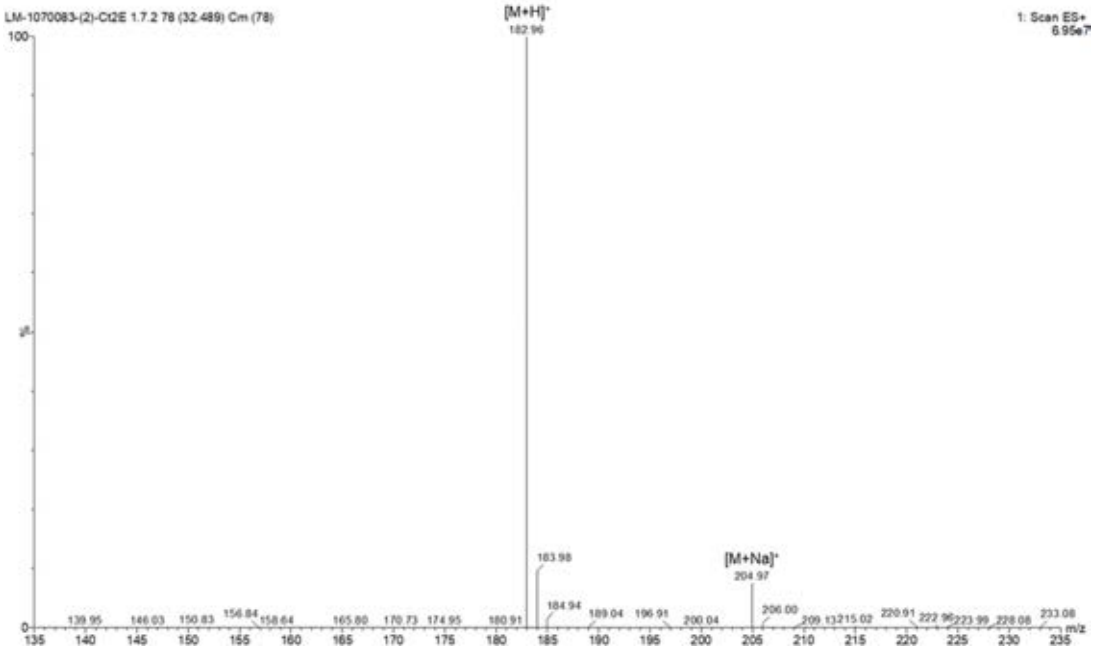

Figure XXXV. ESI-MS spectrum of Ct2E 1.7.2 (**5**)

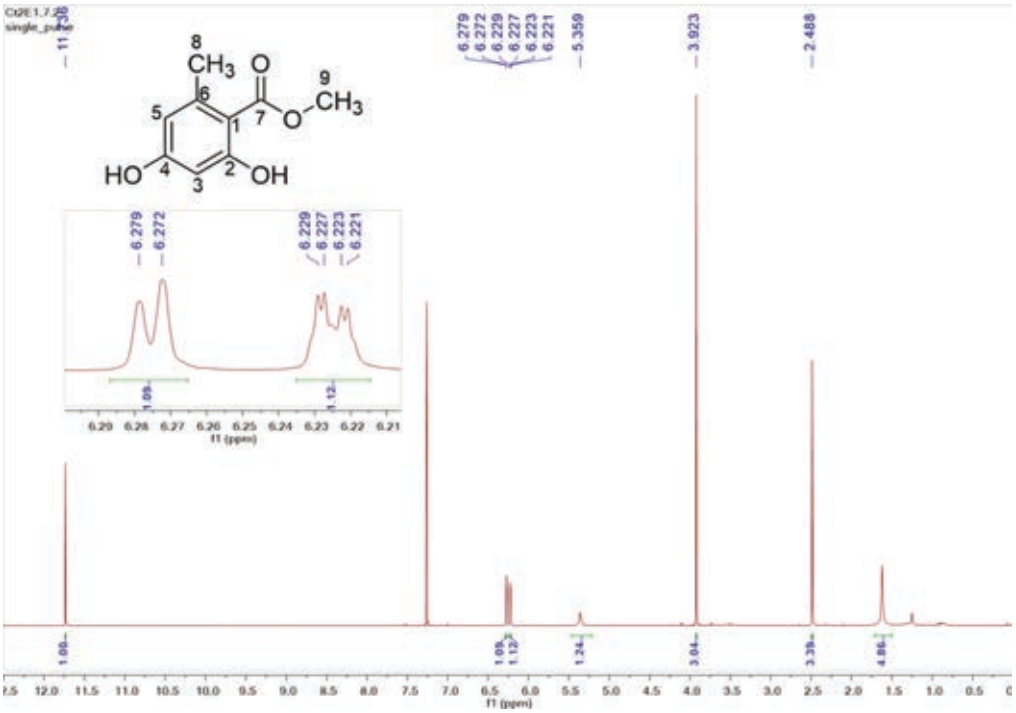

Figure XXXVI. ^{1}H NMR spectrum of Ct2E 1.7.2 (**5**) in $CDCl_3$, 400 MHz

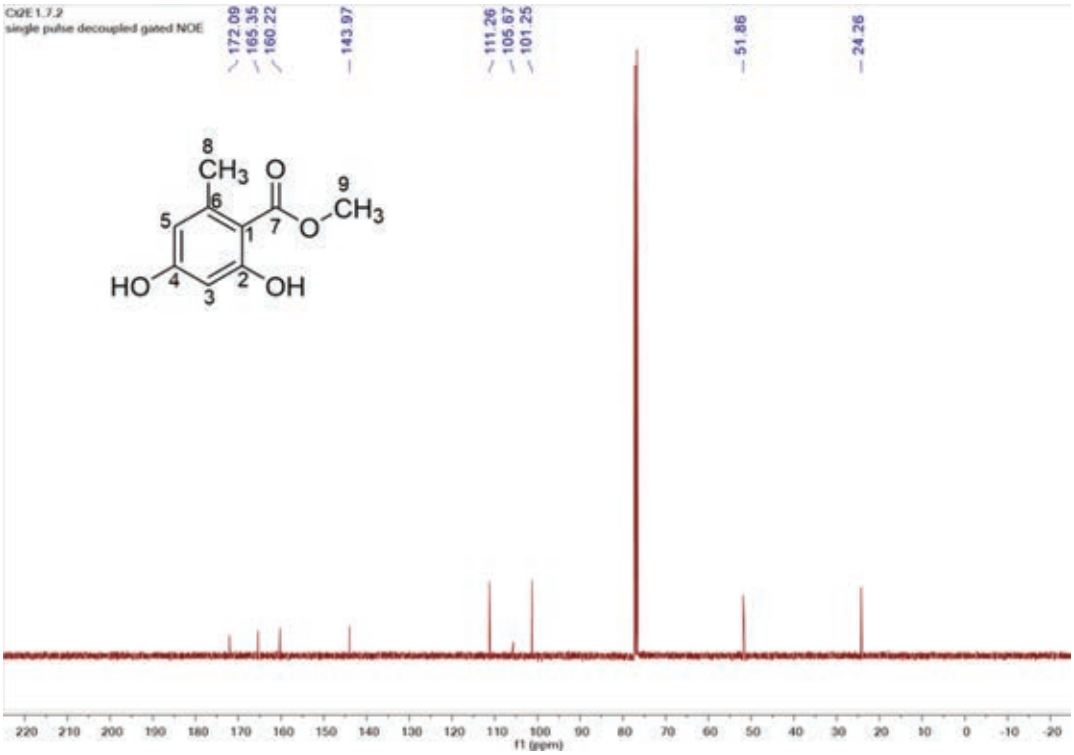

Figure XXXVII. COSY spectrum of Ct2E 1.4.2.1.3 (**4**) (expansion)

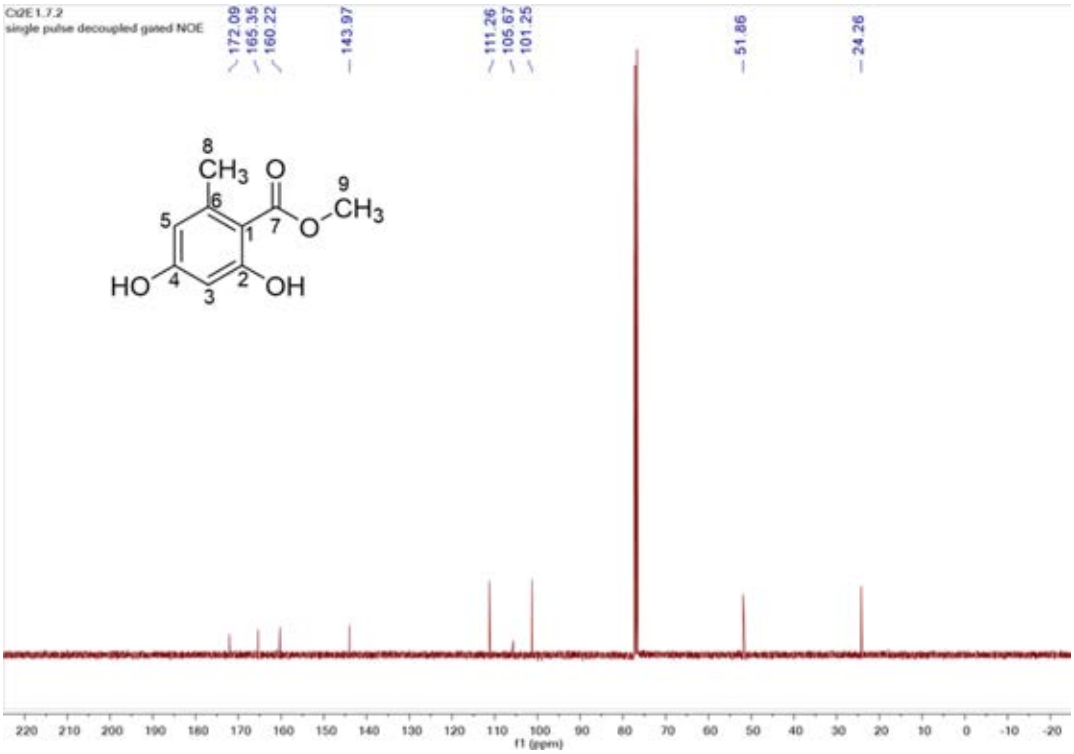

Figure XXXVIII. HMBC spectrum of C2E 1.4.2.1.3 (**4**)

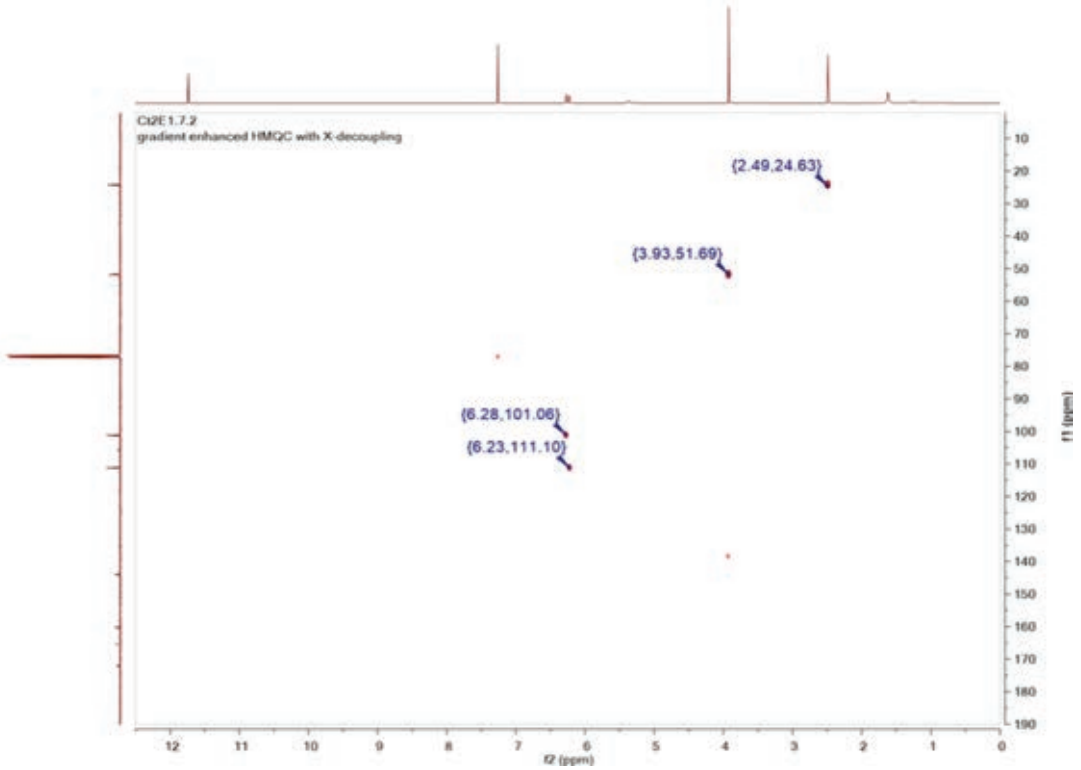

Figure XXXIX. ESI-MS spectrum of Ct2E 1.7.2 (**5**)

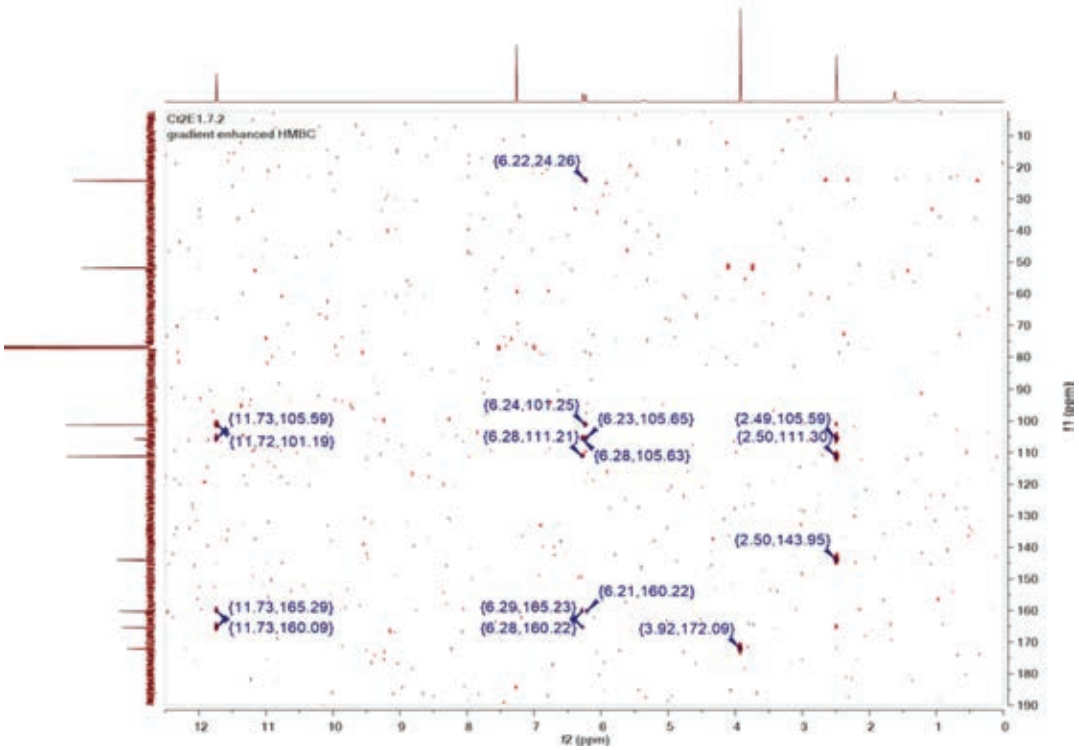

FigureXL. ^{1}H NMR spectrum of Ct2E 1.7.2 (**5**) in $CDCl_3$, 400 MHz